The Microbe 6 (2025) 100269

Contents lists available at ScienceDirect

The Microbe

journal homepage: www.sciencedirect.com/journal/the-microbe

Development of inorganic nanoparticle glycoconjugate enhanced cotton fabrics for multi-drug-resistant *Pseudomonas aeruginosa* bacterium

Ardanur Küçük [a], Zehra Taşdelen [a], Şevval Güney [a], Sedanur Sel [a], Esinti İrem Demirbaş [a], Fatma Öztürk Kırbay [a,b], Sedanur Sancak [a], Maarja Otsus [c], Hafize Dilek Tepe [d], Kaja Kasemets [c], Çetin Kılınç [e], İdris Yazgan [a,*]

[a] Center for Biosensors and Materials, Department of Biology, Faculty of Science, Kastamonu University, Kastamonu, Turkey
[b] Department of Biochemistry, Faculty of Science, Ege University, İzmir, Turkey
[c] National Institute of Chemical Physics and Biophysics, Laboratory of Environmental Toxicology, Tallinn, Estonia
[d] Applied Science Research Center, Manisa Celal Bayar University, Manisa, Turkey
[e] Department of Medical Microbiology, Faculty of Medicine, Kastamonu University, Kastamonu, Turkey

ARTICLE INFO

Keywords:
Antimicrobial cotton fabric
Gold nanoparticle glycoconjugates
Silver nanoparticle glycoconjugates and
Pseudomonas aeruginosa

ABSTRACT

Surface modification of cotton fabrics is required to advance their inherent properties in the development of antibacterial cotton fabric-based biomaterials. In this study, an antibacterial cotton fabric for multidrug resistant *Pseudomonas aeruginosa* species was developed. To do this, lactose and galactose derivatives were used to synthesize silver (Ag) and gold (Au) nanoparticle glycoconjugates (NP-GCs) to functionalize the cotton fabrics to target the carbohydrate binding proteins LecA and LecB lectins found on *P. aeruginosa*. The three lactose derivatives (i.e. Lactose sulfanilic acid (LSA), Lactose 5-aminosalicylic acid (L5AS) and Lactose 4-(4-aminophenyl) butyric acid (L4APB)) gave stable AgNP-GCs and AuNP-GCs while Galactose 4,4'-oxydianiline (GODA) allowed only stable AuNP-GCs synthesis. The cotton fabrics were pretreated to eliminate non-cellulosic parts to obtain scoured cotton fabrics (sCFs) for surface functionalization with AgNP-GCs and AuNP-GCs. Three different approaches (i.e. direct adsorption or adsorption through sulfhydryl group on sCFs and *in situ* synthesis) were followed to obtain AgNP-GCs functionalized cotton fabrics while AuNP-GCs functionalization was performed only through *in situ* synthesis. AgNP-GCs and AuNP-GCs were *in situ* synthesized on the sCFs under heat-treatment, and homogenous surfaces with high load of AgNP-GCs or AuNP-GCs were obtained. AuNP-GC-sCF were then functionalized with Colistin in order to add antibacterial property for *P. aeruginosa*. The colloidal AgNP-GCs, and *in situ* synthesized AgNP-GC-sCF and AuNP-GC-sCF showed strong antibacterial activity for *P. aeruginosa*. The formulations were then tested for gram (-) *Escherichia coli* and *Klebsiella pneumoniae,* and gram (+) *Staphylococcus epidermidis* to evaluate whether they have wide-spectrum antibacterial activity. While the colloidal AgNP-CGs showed similar high toxicity for these species in comparison to *P. aeruginosa*, only LSA_AgNP-GC-sCF and LSA_AgNP-GC-sCF showed 100 % growth suppression for *E. coli*, *K. pneumoniae* and *S. epidermidis*. The Colistin functionalized AuNP-GC-sCFs were also tested for Colistin resistant *K. pneumoniae*, and > 99 % growth suppression was obtained. We also tested whether the surface charge of the AuNP-GCs affect their interactions with *P. aeruginosa* using confocal laser scanning microscopy, where clear interactions were observed for GOD-A_AuNPs. These early results revealed that inorganic nanoparticle glycoconjugates can be designed to develop antibacterial cotton fabrics through designing chemistry that can target lectins on bacterial membranes.

1. Introduction

Bacteria can gain resistance to conventional antibiotics, so today's strong antibiotics will be barely effective in the future, which will weaken the treatment efficiency (Burkatovskaya et al., 2008). It is proposed that bacteria-specific nano-formulations, instead of conventional antibiotics, will be among the best possible options to fight against multi-drug resistant (MDR) bacterial infections (Wang et al., 2020). Among these nano-formulations, inorganic nanostructures (INSs) are the main tools to develop antibiotic-free antibacterial agents against

* Corresponding author.
E-mail address: iyazgan@kastamonu.edu.tr (İ. Yazgan).

https://doi.org/10.1016/j.microb.2025.100269
Received 2 December 2024; Received in revised form 4 February 2025; Accepted 12 February 2025
Available online 13 February 2025

MDR bacterial strains (Wounds and Nowak, 2021). In this perspective, silver nanoparticles (AgNPs) are among the most widely studied INMs because of their strong antibacterial activity (Khan et al., 2018). The antibacterial activities of AgNPs are resulted from a variety of mechanisms including oxidative stress, interference to ATP production, cell wall damage, interaction with nuclear materials and ribosome (Yin et al., 2020). For example, Pareek et al. (2021) showed that AgNPs dysregulated type II fatty acids biosynthesis and caused oxidative stress in MDR *Klebsiella pneumonia* (Pareek et al., 2021). Similarly, AgNPs were shown to impair DNA and accompanying protein synthesis in *P. aeruginosa*, which elevates oxidative stress and biofilm formation (Zhang et al., 2020). Therefore, the antibacterial power of the AgNPs has been transferred to biomedical applications, for instance, nanosilver coated cotton fabrics were used to develop antibacterial surfaces against the antibiotic-resistant bacterial species (El-Shishtawy et al., 2011). Besides the AgNPs, gold nanoparticles (AuNPs) are also convenient INMs used for antibacterial agent development studies as support materials carrying conventional antibiotics. AuNPs provide feasible support for the antibiotics to advance their antibacterial capacity even against the MDR bacterial strains (Sarma et al., 2024), and they can reduce the required amounts to bring out bactericidal effect (Sarma et al., 2024). Both silver nanoparticles (Ullah et al., 2022a, 2022b) and antibiotic functionalized AuNPs can also be used to coat surfaces in order to obtain different biomedical products. In this context, cotton fabrics are attractive base materials (Ghosh, 2021; İpek and Ertekin, 2021) owing to their strong mechanical (Chen et al., 2023a) and water-vapor absorbing characteristics (Chen et al., 2023b) in the development of antibacterial cotton fabrics (Gokce et al., 2020; Li et al., 2023).

Cotton fabrics (CFs) are mainly composed of cellulose (95 % (Knežević et al., 2022)) along with such impurities including waxes, pectin and proteins as of non-cellulosic components (Chung et al., 2004). It is the most abundant cellulosic material used in the textile industry (Knežević et al., 2022; Dang et al., 2024). Cellulosic materials provide unique platforms for nanomaterial introduction in a variety of applications (Gulati et al., 2022; Khan et al., 2017), including antibacterial fabrics (Raw and Fiber, 2023; Soleimani-Gorgani et al., 2023), UV protective fabrics (Nosheen et al., 2022), inflammable fabrics (Attia et al., 2023) and face-masks (Mast et al., 2023). Functionalization of CFs to advance the antimicrobial properties are mainly performed by introduction of nanomaterials and bioactive compounds (Shehabeldine et al., 2022). For example, silver/zinc doped cotton/paraffin (Wang et al., 2024) and amoxicillin loaded cellulose based composite (Qi et al., 2024) wound dressing fabric brought out broad antibacterial activity while contributing wound healing. The improved antimicrobial activity relies on a variety of mechanisms including controlled release of biocides, repulsion of microorganisms (e.g. via controlled hydrophobicity, electrostatic repulsion, alteration in surface topography and energy etc.) and capture of microorganism (for details (Muhammad et al., 2024)). For example, chitosan-zinc nanostructure introduced CFs possessed strong antibacterial capacity against both gram (+) and gram (-) bacterial species (AbdElhady, 2012). Similarly, copper oxide nanostructures (Nanoparticles, 2020; Wang et al., 2023), silver oxide nanoparticles and titanium oxide nanoparticles (Gao et al., 2021), titanium doped silver nanoparticles (El-Naggar et al., 2022) silver nanostructures (Raw and Fiber, 2023; Soleimani-Gorgani et al., 2023) were shown to be excellent nanomaterials advance the antimicrobial capability of CFs. Despite of the fact that successful applications of impregnation of pre-synthesized nanostructures onto cellulose based fabrics (Hu et al., 2024), *in situ* synthesis of AgNPs (Wu et al., 2024) and AuNPs (Anwar et al., 2021) onto the cotton fabrics to obtain functional and antimicrobial biomedical materials in order to provide a homogenous surface.

Pseudomonas aeruginosa is a motile rod-shaped biofilm-forming gram (-) and non-sporous bacterium that causes opportunistic infections (Pina-Sánchez et al., 2023). The life-threatening infections of *P. aeruginosa* are mostly related to such diseases as pulmonary infections, urinary tract infections, burn wounds, and cystic fibrosis (Belgin and Öz, 2017). Since it develops resistance to antibiotics, the treatment and choice of antibiotics are not trivial (Pina-Sánchez et al., 2023). Particularly, MDR *P. aeruginosa* is listed as the greatest problematic bacterial species (Azam and Khan, 2019). Targeting LecA/LecB lectins are among the current approaches to eliminate MDR *P. aeruginosa* infection. Lectins are specific proteins that recognize free and/or bound carbohydrate residues on/in cells (Behzadi et al., 2021; Hu et al., 2019). LecA (Yu et al., 2019) and LecB (Sommer et al., 2014) selectively binds to lactose, galactose and fucose residues (Hu et al., 2019), and they have medicinal interest to prevent *P. aeruginosa* attachment to lung cells (Pertici and Pieters, 2012; Loris et al., 2003). However, to the best of our knowledge, this knowledge has not been transferred to the development of antimicrobial cotton fabric relying on carbohydrate-lectin interactions. In this study, we synthesized three lactose and one galactose derivatives that were used in the synthesis of silver and gold nanoparticle glycoconjugates, which were then introduced to scoured cotton fabric or used *in situ* synthesis of AgNP-GCs-sCF and AuNP-GCs-sCF. Due to the fact that AgNPs are potent antibacterial agents (Yaman Turan et al., 2024), AgNP-GCs-sCFs were used as synthesized while the antibiotic Colistin (targeting gram negative bacterial species (Elias et al., 2021)) was used to functionalize AuNP-GCs-sCF to have antibacterial surfaces. The carbohydrate ligands served as recognition elements to capture bacterial species (Kumar et al., 2019), which improves the contact of AgNPs and Colistin to the bacterial cells. The developed materials were characterized by spectroscopic, microscopic and microbiological techniques. The findings showed that the AgNP-enhanced cotton fabrics and Colistin-modified AuNPs-enhanced cotton fabrics gave excellent antibacterial activity against *P. aeruginosa* and the other tested other gram (-) and gram (+) bacterial species.

2. Material and methods

2.1. Materials

Raw cotton fabric and viscous bleach (active chlorine content <5) were purchased from a local store. Mueller Hinton Broth, sulfanilic acid (99 %), lactose monohydrate (microbiology grade), 5-aminosalicylic acid (99 %), 4-(4-aminophenyl) butyric acid (%95), Galactose (≥99 %), 4,4'-oxydianiline (97 %), borane dimethylamine complex (97 %), Mueller Hinton Agar, $AgNO_3$ (≥99.0 %), anhydrous acetone, 200-proof ethanol (≥99.5 %, ACS reagent) and sodium hydroxide pellets were purchased from Sigma-Aldrich. 18.2 MΩ pure water was obtained using the Humana Zeneer water purification system in our labs.

2.2. Scouring cotton fabrics

In order to prevent possible damage to the fibers of the cotton fabric during the scouring, mild conditions were used as described in the literature (Yiğit et al., 2021). 2:98 (v/v) commercial viscous bleach was applied to 400 cm^2 cotton fabric at room temperature for overnight. The whitened cotton fabric was soaked into 2 % aqueous NaOH (w/v) for 2 h at 60 °C in order to eliminate non-cellulosic components (Rezaee et al., 2021). IR spectroscopy is a sensitive technique to monitor chemical alteration on surfaces (Chung et al., 2004), so the treated cotton fabrics were monitored using ATR-FTIR spectroscopy (Bruker Alpha II ATR-FTIR).

2.3. Synthesis and characterization of silver and gold nanoparticle glycoconjugates

In the first step, lectin databases were used to find out relevant publications revealing possible lactose and galactose derivatives that can be used to target *P. aeruginosa* (Supplementary Material **Section 1**). The sugar ligands were synthesized using reductive amination method as detailed in literature (Saladino et al., 2021; Jeong et al., 2007) (Supplementary Material **Section 2**). The synthesis of AgNPs was simply

performed by mixing the sugar ligands and silver nitrate in pure water for up to 6 h incubation at room temperature to obtain stable AgNPs. This approach allows fast and stable inorganic nanomaterial synthesis as shown previously by our group (Yazgan et al., 2020, 2021). It is also known that carbohydrates can also allow synthesis of stable AgNPs (Khan et al., 2018), where they can serve as reducing, capping and stabilizing agent. The molar ratios of the sugar ligands to silver nitrate were 7.23, 3.61, 1.82, 0.91 and 0.45, so the AgNPs were named AgNP7.23, AgNP3.61, AgNP1.82, AgNP0.91 and AgNP0.45. In the case of AuNPs, colloidal golds were only synthesized using L5AS and GODA sugar ligands with 7.23 molar ratio of the sugar ligand to auric acid. Selection of the sugar ligand/metal ion molar ratio was based on our previous studies (Yazgan et al., 2020; Sancak et al., 2023a). GODA sugar ligand did not provide any stable AgNPs under the tested conditions.

UV–vis spectroscopy (Multiskan SkyHigh Microplate Spectrophotometer, Thermofisher Scientfic) at 350–900 nm range was used to characterize surface resonance peaks of the nanoparticles while high-resolution transmission electron microscopy (TEM) (FEI TALOS F200S TEM 200 kV, Thermofisher Scientific, service was purchased from BUMER-Bayburt University) was used to characterize the morphology and crystal structure. ATR-FTIR (4000–400 cm^{-1}) (ALPHA II Compact FT-IR Spectrometer, Bruker) was used to characterize the sugar ligand-AgNPs interactions.

2.4. Preparation and characterization of cotton fabric nanoparticle glycoconjugate composites

In the case of silver nanoparticle enhanced cotton fabric production three different approaches were followed (Fig. 1). (i) 5 mL of the selected AgNPs (1.26 mg/mL Ag content) were dropped on the scoured CFs (sCFs) or Cysteine modified sCFs (Cysteine introduction was performed based on the procedure given in the literature (Bayisa et al., 2023)) followed by keeping in an air-tight glass chamber at room temperature for 6 h or 2 h under 50 ºC treatment. Right after the incubation, the coated CFs were vortexed in pure water twice to eliminate unbound AgNPs. In the second approach (ii), the scoured cotton fabric silver and gold nanoparticle glycoconjugates were obtained through *in situ* AgNPs or AuNP synthesis on the scoured cotton fabrics. Briefly, the sugar ligand was added to the sCF and incubated for 10 min to allow sCF to fully absorb the sugar ligand. Then $AgNO_3$ (2 mg/mL) or $HAuCl_4{\cdot}3(H_2O)$ (0.8 mg/mL) dissolved in 5 mL was added to the sugar ligand containing sCF and incubated in a sealed glass contained at 50 °C for 6 h. The molar ratios were 0.91 and 3.61 for L5AS/Ag^+, and LAPA/Ag^+ and LSA/Ag^+ while it was 7.23 for all of the AuNP-GC-sCFs. After the incubation, the sCF-AgNPs were rinsed twice with excess water. The coated CFs were then immersed in 70 % ethanol, followed by dried in a Biosafety Level 2 cabinet. The dried CF-AgNPs were exposed to 254 nm UV light for 30 min. The sterilized coated-CFs were characterized using leakage test (UV–vis spectroscopic test), total volume (BET), ATR-FTIR and SEM-EDX (FEI Quanta FEG 250) techniques, and microbiological tests. In the case of AuNP-enhanced cotton fabric preparation, only the third approach was followed with the same concentrations, for which SEM-EDX (FEI Quanta FEG 250) and microbiological tests were performed for the characterizations.

2.5. Microbiological characterizations of the AgNPs and coated cotton fabrics

All the studied AgNPs were tested for their antibacterial activities as described in the literature using Nutrient Broth and Nutrient Agar (Saladino et al., 2021). As of the first step, AgNPs were tested for their toxicity against *P. aeruginosa* (gram -) using minimum inhibitory (MIC), minimum bactericidal (MBC), and biofilm formation tests. *Escherichia coli* (gram -), *Klebsiella pneumoniae* (gram -), *Staphylococcus epidermidis* (gram +) were used to test the selectivity of the AgNPs. It should be noted that the all gram negative bacterial species were resistant to Colistin while *S.epidermidis* was resistant to Pencillin G (MIC values were >10 µg/mL). MIC and MBC values were found using the serial dilution method (Sancak et al., 2023b) and the alterations in biofilm forming capacity of the bacterial species were tested at different AgNPs doses.

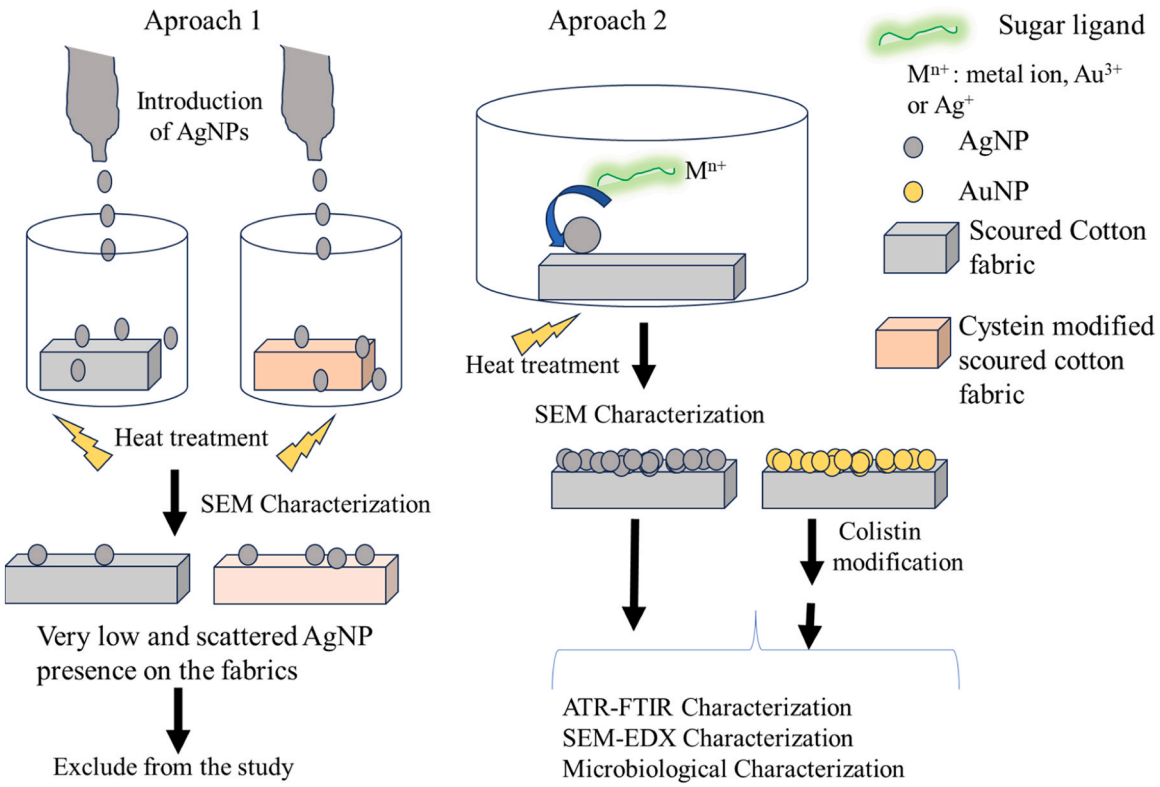

Fig. 1. Nanoparticle cotton fabric production approaches.

The antibacterial capacity of the AgNP-GC-sCFs and Colistin functionalized AuNPs-GC-CFs was tested by introducing them on freshly prepared agar, allowing them to submerge into the agar. This approach allows for monitoring if the bacterial cells pass through the pores of the developed fabric in comparison to the cotton fabric that was not coated with nanoparticles. 10^6 cfu/20 μL of the bacteria colonies were then introduced on the developed fabrics. Bacterial growth was checked right after an overnight incubation (16–18 h period). After the incubation, the cotton fabrics were placed into sterile tubes containing 5 mL of pH 7.4 PBS buffer and rinsed three times under 600 rpm vortexing. The developed cotton fabrics were then placed in 5 mL of broth and then incubated for 16 h. The turbidity of the samples was then read at 595 nm to monitor propagation of *P. aeruginosa* cells localized in/on the formulated cotton fabrics (Fig. 2).

The interaction between AuNP-GCs (i.e. GODA_AuNP-GC and L5AS_AuNP-GC, which are the two highly charged AuNPs) and *P. aeruginosa* was evaluated using confocal laser scanning microscopy (CLSM). For CLSM, bacteria *P. aeruginosa* ATCC 27853 from an exponentially growing culture in Luria-Bertani medium were washed twice by centrifugation (10 min, 5094 g; Sigma 3–16PK, Germany) with DI water and resuspended in DI water ($OD_{600\ nm} = 0.5$; ~10^6 cell forming units/mL) and exposed to the studied NPs at 5 mg/L for 1 h at room temperature. After the incubation, the cell suspension was stained by 5 μM Syto9 (InvitrogenTM Thermo Fisher Scientific, USA) for 10 min in the dark. 20 μL of the stained cell suspension was then spread on the microscopy slide, dried at 37 °C for 15 min and mounted in Mowiol (Sigma-Aldrich, Germany). The samples were visualized with Zeiss LSM800 CLSM (Zeiss, Jena, Germany) using a 488 nm laser and 505–550 nm emission filter to acquire a Syto9 signal. Nanoparticles were visualized by reflection mode at 640 nm. Images were processed using ZEN software (Carl Zeiss Microscopy, Jena, Germany).

3. Results and discussions

3.1. Structural characterizations of the sugar ligands, nanoparticle glycoconjugates and nanoparticle glycoconjugate-cotton fabric formulations

3.1.1. ESI-MS/MS characterization of the carbohydrate derivatives

ESI-MS/MS fragmentation pattern of LSA, L5AS, and L4APB were monitored using acetic acid/water (20:80, v/v) as the solvent, where protonation could add protons to the amino groups in addition to the proton came from positive screening mode. Therefore, we chose ± 2 *m/z* during the screening in order to get reliable result (Yazgan, 2019). The fragment pattern showed that losses of 162 *m/z*, 180 *m/z* and 198 *m/z* were common in LSA, L5AS and L4APB. The loss of 162 *m/z*, 180 *m/z* could refer to galactose moiety cleavage were in the form of pentose and hexose moiety, respectively. The loss of 198 *m/z* could be related to elimination of the water group right after the galactose moiety (as hexose) since it is common in all of them. In LSA and L5AS, the loss of 216 *m/z* also refers to one more -H_2O elimination. Besides, the loss of 261.95 *m/z* (180.05 + 81.08 *m/z*) refers to the loss of the sulfonyl group accompanied by galactose moiety loss in LSA. GODA was also characterized using negative mode ESI-MS, and 526 *m/z* was found (Supplementary Material **Section 2**).

3.1.2. Infrared spectra analyses of the reactants

In the IR spectroscopic characterizations, the monomers and the possible residual contaminant sodium acetate should be analyzed. In the sodium acetate IR spectrum (Supplementary Material **Section 3**), the peaks at 3407 cm^{-1}, 3277 cm^{-1}, and 3165 cm^{-1} are from the hydration of the carboxylate group with different hydration (Pitch et al., 2015) and protonation levels. The peak at 2981 cm^{-1} is from asymmetric CH_3 stretching while the peak at 1015 cm^{-1} and 1049 cm^{-1} are from CH_3-C stretching and CH_3-C-O stretching accompanied with in-plane CH_3 rocking, respectively (Kakihana and Nagumo, 1987). The peaks at 1545 cm^{-1} and 1406 cm^{-1} belong to asymmetric and symmetric COO, respectively (Kakihana and Nagumo, 1987; Habka et al., 2019) while the peaks at 634 cm^{-1} and 510 cm^{-1} are from COO bending and in-plane COO rocking (Kakihana and Nagumo, 1987). The two adjacent peaks at 1696 cm^{-1} and 1635 cm^{-1} are possibly related to the carbonyl functional group of carboxylate moiety (Susan Doofan et al., 2021). The peaks at 925 cm^{-1} and 795 cm^{-1} belong to COO-C stretching and CH_3 rocking, respectively (Kakihana and Nagumo, 1987).

5-aminosalicylic acid (5AS) IR spectrum (Fig. 2) reveals the presence of the bands belonging to C-H stretching (2770 cm^{-1}), intramolecular hydrogen bonding with a carboxylic group (2492 cm^{-1}), C═O stretching of carbonyl group (1664 and 1572 cm^{-1}), N-H bending (1612 cm^{-1}), C═C stretching of aromatic group (1484 cm^{-1}), bending of -OH of carboxyl group (1444 cm^{-1}), Ar C-N stretching (1347 cm^{-1}), -OH stretching (1084 cm^{-1}) and C-H out of plane bending (808–706 cm^{-1}) (Hu et al., 2012; Singh et al., 2007).

Due to the fact that sugars give very strong IR peaks in the range of 4000–400 cm^{-1} and most of them are common in disaccharides and monosaccharides (Wiercigroch et al., 2017), we only focused on the characteristic glucose and galactose moieties to monitor the synthesis of lactose derivatives and their introduction to scoured cotton fabric in the form of sugar ligand-silver nanostructures (Supplementary Material **Section 3**). The following peaks belong to glucose unit of lactose, including 3521 cm^{-1} (stretching OH), 1256 cm^{-1} (rocking CH and OH), 1166 cm^{-1} (stretching CO), 1064 cm^{-1} (stretching CC), 1028 cm^{-1} (symmetric stretching CC), 755 cm^{-1} (twisting CO, COHO and HOH), 547 cm^{-1} (in-plane bending OCO), 466 cm^{-1} and 439 cm^{-1} (in-plane bending CCO). The characteristic galactose unit of lactose peaks are

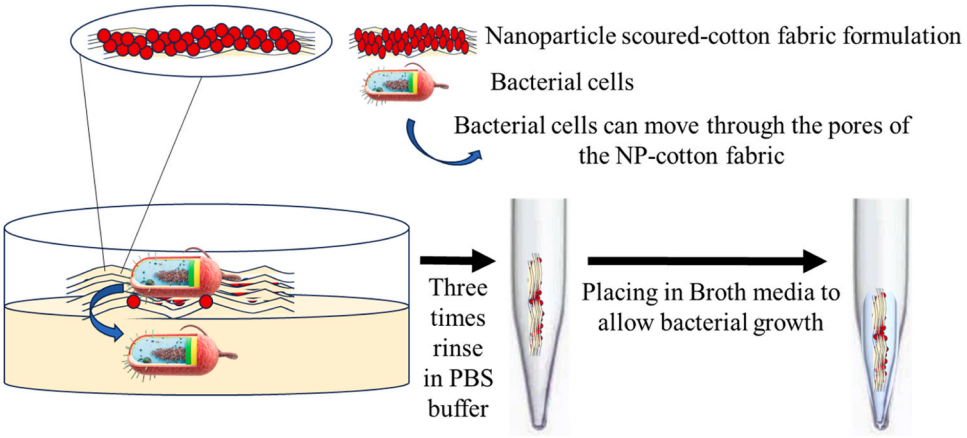

Fig. 2. Antibacterial activity testing flow of nanoparticle cotton fabric formulations.

1421 cm^{-1} (wagging CH_2), 1201 cm^{-1} (in-plane bending OH and rocking CH_2), 1103 cm^{-1} (stretching CO), 673 cm^{-1} (in-plane bending CCO) and 601 cm^{-1} (in-plane bending OCO) (Wiercigroch et al., 2017).

Characteristic peaks belonging to 4ABP are 2997 cm^{-1} O-H stretching, 2530 cm^{-1} alkyl C-H vibration, 2385 cm^{-1} CO_2 stretching, 1575 cm^{-1} NH_2^+ deformation, 1418 cm^{-1} CH_2 bending, 1374 cm^{-1} C═O stretching, 1279 cm^{-1} Ar C-N stretching, and 1203 cm^{-1} CH_2 twisting vibration bands. The peak at 1203 cm^{-1} belongs to CH_2 twisting vibration while the peak at 1016 cm^{-1} and 924 cm^{-1} are from the aromatic ring and overlaps from the aromatic ring, CH_2 and CC bonds, respectively. Besides, the wagging of NH_2 group contributed to the peaks at 554 and 592 cm^{-1}. However, a strong carbonyl band peak at ~1720 cm^{-1} and a medium NH_2 deformation band peak between 3200 and 3400 cm^{-1} range were not observed for this molecule because of the fact that inter- and intra-molecular hydrogen bonding occurred between carboxyl and amino group. Besides, amino peaks can couple with CC bond and CH vibrations of the phenyl ring, so the expected peaks become unclear (Akkaya et al., 2015) (Supplementary Material **Section 3**).

Sulfanilic acid undergoes dimerization, and its functional groups interact with each other even in solid form. Therefore, its IR spectrum might not provide all the expected groups when the IR analysis is performed at room temperature. Hereby, we assigned the characteristic peaks including O-H stretching band (2873 cm^{-1}), C-H stretching (2635 cm^{-1}), NH_2 scissoring (1627 cm^{-1}), NH_3 symmetric bending (1495 cm^{-1}), vibration from phenyl ring (1418 cm^{-1} and 1004 cm^{-1}), C-N stretching (1239 cm^{-1}), in-plane bending of C-H and rocking NH_2 of SA dimer (1111 cm^{-1}), NH_2 rocking (1033 cm^{-1}), and SO_2-OH asymmetric bending of SA dimer (500 cm^{-1}) (Srimathi et al., 2014) (Fig. 2). Based on these assignments, it can be concluded that sulfanilic acid powder is in zwitterionic and dimer forms (Srivastav et al., 2023). Particularly, the peaks belonging to NH_2 and Ar C-N bands are critical to monitor the successful substitution of sulfanilic acid to carbohydrates.

3.1.3. *Infrared spectra analyses of the carbohydrate derivatives*

In order to simplify the interpretation, the IR spectra of the sugar ligands are, here, discussed together (Fig. 3). It is noteworthy to mention that the sugar moiety tends to bend over the aromatic substituted group for these types of ligands (Yazgan et al., 2021), so the characteristic peaks of galactose moiety are not expected to give shifts at exactly the same wavenumber as they are seen in pure-lactose. Upon sugar ligand formation, a strong wide shift lying between 3660 and 3020 cm^{-1} with a peak at 3328 ± 4 cm^{-1} belonging to -OH stretching concealed the three peaks of lactose at ~3521 cm^{-1}, 3324 cm^{-1}, and 3241 cm^{-1}. The peak at 2909 ± 11 cm^{-1} belongs to -CH_2 vibration of lactose moiety of the ligands as well. The peaks at 890 cm^{-1}, 896 cm^{-1}, and 892 cm^{-1} can be assigned to galactose moiety (Wiercigroch et al., 2017) of LSA, L5AS, and L4APB ligands, respectively. The peak at 1272 cm^{-1} belongs to the rocking or bending vibration of CH and OH groups in the LSA spectrum while those appeared at 1249 cm^{-1} and 1252 cm^{-1} in L5AS and L4APB spectra, respectively. It is essential to bear in mind that certain IR peaks from self-dimerized sulfanilic acid seen in SA IR spectrum (Srivastav et al., 2023) will not be visible in LSA IR spectrum due to the fact lactose moiety alters SA-SA interactions through excess -OH groups along with that lactose moiety bends over the phenyl ring (Yazgan et al., 2021), so we paid effort to specific peaks related to aromatic ring, sulfonyl group and the secondary amine group of LSA. The peaks belonging to zwitterion and dimeric forms of SA along with NH_2 rocking are not present in LSA while vibration from SO_3H (sulfur-oxy) at 1404 cm^{-1} is present in LSA (Rana Tomar and Venkatesan Jayakumar, 2023). The peak at 1599 cm^{-1} could be from ArC=N while the peak at 1519 cm^{-1} belongs to vibration from the aromatic ring (Ismail et al., 2014) in LSA. However, the peak at 1599 cm^{-1} is quite sharp, so it could be resulted from the aromatic ring as well. The peaks at 1156 cm^{-1}, 1117 cm^{-1}, 1067 cm^{-1}, 831 cm^{-1}, 700 cm^{-1} and 557 cm^{-1} belong to ArC-N-C stretching, SO_2 symmetric stretching, S-O(H) mode vibration, aromatic ring vibration and SO_2-OH asymmetric bending, respectively. Besides, CH_2 bending at 1466 cm^{-1}, CH/OH rocking/bending vibration at 1272 cm^{-1}, galactose ring torsion at 779 cm^{-1} and galactose bending

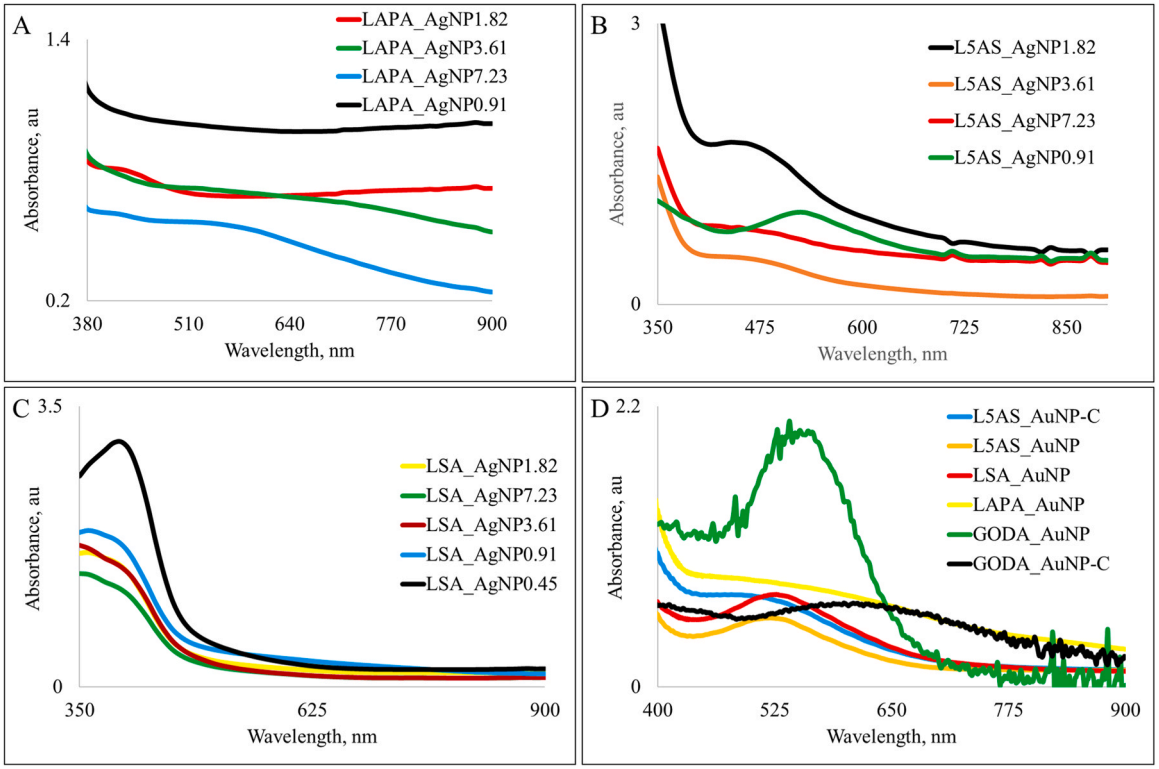

Fig. 3. UV-Vis spectra of LAPA (A), L5AS (B) LSA (C) synthesized colloidal AgNPs, and AuNPs and Colistin functionalized AuNPs (D).

vibration at 626 cm^{-1} in the LSA spectrum belong to lactose residue. The galactose ring torsion peaks of L5AS and L4APB showed up at 784 and 785 cm^{-1}, respectively. In the L5AS spectrum, carbonyl group vibration (e.g. stretching) showed up at 1665 and 1626 cm^{-1} while -OH bending of the carboxyl group and ArC-N stretching bands showed up at 1422 cm^{-1} and 1319 cm^{-1}, respectively. The vibrations (e.g. C═C bending, C═C-H stretching) from the aromatic group of L5AS gave peaks at 1493, 830 and 701 cm^{-1}. The carbonyl group gave vibration at 1705 cm^{-1} in addition to the stretching carbonyl band at 1392 cm^{-1} in L4APB. The peaks at 1467 cm^{-1} and 1142 cm^{-1} belong to N-H bending and ArC-N-C stretching, respectively. Aromatic ring vibration (e.g. 1550 cm^{-1}) and alkyl C-H vibration peaks appeared between 810 and 432 cm^{-1} in L4ABPB. Through monitoring the peaks at 925 and 795 cm^{-1} belonging to acetate, it was cleared that the sugar ligands did not contain acetate residue (Supplementary Material **Section 3**).

3.1.4. Infrared spectra analyses of the cotton fabrics

ATR-FTIR spectroscopy allows monitoring the changes on the surfaces, and successful applications were shown for the scoured cotton fabrics (Chung et al., 2004). Non-cellulosic components reside in different layers of cotton fabric (Colombi et al., 2021), we monitored entire IR spectrum to check whether any band belong to pectin and/or wax remained in the cotton fabric. The wide -OH stretching band lied between 3620 and 3000 cm^{-1} in raw cotton fabric (rCF) shifted to 3620–3044 cm^{-1} range in the scoured cotton fabric (sCF). The -OH stretching band revealed its presence with two discernible peaks at 3332 and 3271 cm^{-1} in sCF spectrum while there was not a discernible peak in rCF spectrum. Similarly, the -CH_2 vibration peaks at 2914 and 2850 cm^{-1} in rCF shifted to 2969 and 2897 cm^{-1} in sCF spectrum. The shift reveals that wax was removed from the cotton fabric since the peaks at 2914 and 2850 cm^{-1} are from wax (Chung et al., 2004). There was no peak for the carbonyl group representing the carbonyl group from pectin in rCF and sCF spectra. However, sharper C-O-C, -OH, CH, and C-O vibration bands got relatively sharper and stronger, so it can be claimed that the scouring was successful (Figure was not shown).

IR spectra of the bleached and raw cotton fabrics were compared, and no difference was obtained. This is because raw cotton fabric is mostly formed from cellulose, and bleaching only removes such impurities as wax, residual proteins, and organic compounds. However, as it seen from Supplementary Material **Section 3**, bleaching enhanced the IR bands upon removal of the impurities. 3281 cm^{-1} band peak protonated OH stretching, 2910 cm^{-1} C-H stretching, 1427 cm^{-1} CH_2 wagging, 1317 cm^{-1} C-H wagging, 1158 cm^{-1} C-O-C pyranose ring and 1023 cm^{-1} C-O-C stretching (Nateghi and Hajimirzababa, 2014; Sadanand et al., 2017). Physical adsorption of water molecules caused the formation of the broad band between 3500 and 3100 cm^{-1} along with that of the peak at 1610 cm^{-1} (Igarashi et al., 2020). The peaks at 1105, 662, and 602/502/436 cm^{-1} are related to β-glycosidic bond, H-bonded OH and CCC/COC glycosidic bonds, respectively (Wiercigroch et al., 2017; Nikonenko et al., 2005).

The IR spectra of the sugar ligands did not show any dramatic changes upon silver nanoparticle (AgNP) formation (Fig. 3) and the corresponding sCF-AgNP (Supplementary Material **Section 3**). In all cases H- bonded -OH deformation peak at 3666 cm^{-1} became clearer in the AgNPs, which appeared in the corresponding sCF-AgNP. The -OH stretching peaks at 3332 and 3271 cm^{-1} in sCF became weaker upon AgNPs introduction while -CH_2 asymmetric and symmetric became stronger and sharper in the AgNPs and they became even stronger peaks than those obtained for -OH vibrations in sCF-AgNPs. The other clear difference was that the peaks at 1052 and 1026 cm^{-1} in sCF spectrum turned into a stronger and shaper peak at ~1050 cm^{-1} in the sCF-AgNPs in all cases. However, there were not any other major changes, or any characteristic peaks were observed for LSA, L5AS or L4APB sugar ligands in the sCF-AgNPs. When similar studies were conducted for the sCF-AuNPs, no characteristic bands were observed for the sugar ligands as well (data not shown).

3.2. Characterizations of AgNP-GCs and AuNP-GCs

UV-Vis spectroscopic characteristics of the nanoparticles revealed that decrease in sugar ligand/Ag^+ ion ratio resulted in weaking of characteristic SPR peak for LAPA_AgNPs; LAPA_AgNP7.23, LAPA_AgNP3.61 and LAPA_AgNP1.82 gave SPR peaks at 550, 530 and 440 nm while LAPA_AgNP0.91 did not give any SPR peak, which could be related to at this ratio the AgNPs are not stable enough. In the case of L5AS ligand, L5AS_AgNP7.23, L5AS_AgNP3.61, L5AS_AgNP1.82 and L5AS_AgNP0.91 gave SPR peaks at 470, 480, 460 and 530 nm, respectively. The first two SPR peaks are not sharp, which could be related to the fact that they are very small. In contrast to these, LSA synthesized AgNPs gave SPR peak at ~400 nm with an increasing intensity in response to decreasing LSA ligand/Ag^+ ion molar ratio. Colloidal AuNPs gave SPR peaks at 523, 563, 542 and 570 nm for L5AS_AuNP, LSA_AuNP, GODA_AuNP and LAPA_AuNP, respectively. In order to show that Colistin can bind to AuNPs, GODA_AuNPs and L5AS_AuNPs were selected since they have the highest positive and negative zeta potentials; the zeta potentials were −34, −24, 4 and 34 mV for L5AS_AuNP, LAPA_AuNP, LSA_AuNP and GODA_AuNP, respectively. GODA sugar ligand did not provide stable AgNPs under the tested conditions. Colistin functionalization (100 ng Colistin/1 mg AuNP) altered the UV-Vis spectra pattern and SPR peak of GODA_AuNPs (SPR peak shifted from 596 to 632 nm) and L5AS_AuNPs (SPR peak shifted from 523 to 520 nm). Since Colistin was introduced to the media one hour after the nanoparticle synthesis started, it is possible that Colistin also affected the reaction kinetic and nanoparticles' morphologies, and it is known that Colistin can bind to both positively and negatively charged gold nanoparticles (Fuller et al., 2020).

HRTEM-SAED characterizations were performed for selected AgNPs in order to show how the sugar ligand/Ag^+ ion molar ratio and the ligand's chemistry affected morphology and size. L5AS_AgNP0.91 nanostructures are anisotropic and generally pentagonal and minor hexagonal shaped with 67 nm to 234 nm rounded edges while mostly the edges are between 140 and 170 nm. L5AS_AgNP3.61 are a mixture of anisotropic 0D and 1D nanostructures (Fig. 4). Anisotropic AgNPs were sized between ~65 nm and 132 nm while curved 1D structures were up to ~650 nm in length and 112 nm in width.

Sizes between 1.7 and 18 nm with overwhelmingly ellipsoid morphology, and an average of 8.2 nm. ~50 % 5 ± 1 nm range (Fig. 5). SAED analysis showed that the crystalline structure fits to *face centric cubic* lattice (Yazgan et al., 2020). The inset in Fig. 7**B** reveals that the nature of crystallinity has only one direction.

LSA_AgNP3.61 gave no dominant size distribution with ellipsoid to irregularly shaped AgNPs while a minor portion of the AgNPs showed ellipsoidal morphology (Fig. 6). The general range of the AgNPs' edges ranged between ~20 nm and ~190 nm. In contrast to this, LSA_AgNP0.45 gave mostly ellipsoidal-like morphology with edges between 18 and 190 nm. Besides, some spherical and irregularly shaped anisotropic morphology were observed as well (Fig. 6). It is noteworthy that electron-beam triggered AgNPs were also formed within the grid (data not shown), which was not present for LSA_AgNP2 sample. This shows that some of the Ag^{+1} ions did not turn into AgNPs, but interestingly they could not be separated from the mixture using centrifugation (4000 *g* for 10 min). This is probably related to the formation of large and continuous LSA-Ag^+ ion interaction.

Selected area diffraction (SAED) patterns of the AgNPs show that L5AS (Fig. 4) and LAPA (Fig. 5) sugar ligands directed face centric cubic lattice with (111), (200), (220), (311) and (31) miller indices (Reference code: 00–001–1167) (Sancak et al., 2023b). In contrast to these, LSA triggered formation of hexagonally packed crystalline lattice structure (Reference code: 01–087–0598) (Fig. 6), which can co-exist with *fcc* even though the crystal structure is overwhelmingly *fcc* (Virgen-Ortiz et al., 2015). Smaller LSA_AgNPs were in the form of polycrystalline and larger ones were single crystalline. However, it should be noted that SAED pattern of LSA_AgNP0.45 looked like crystalline phases

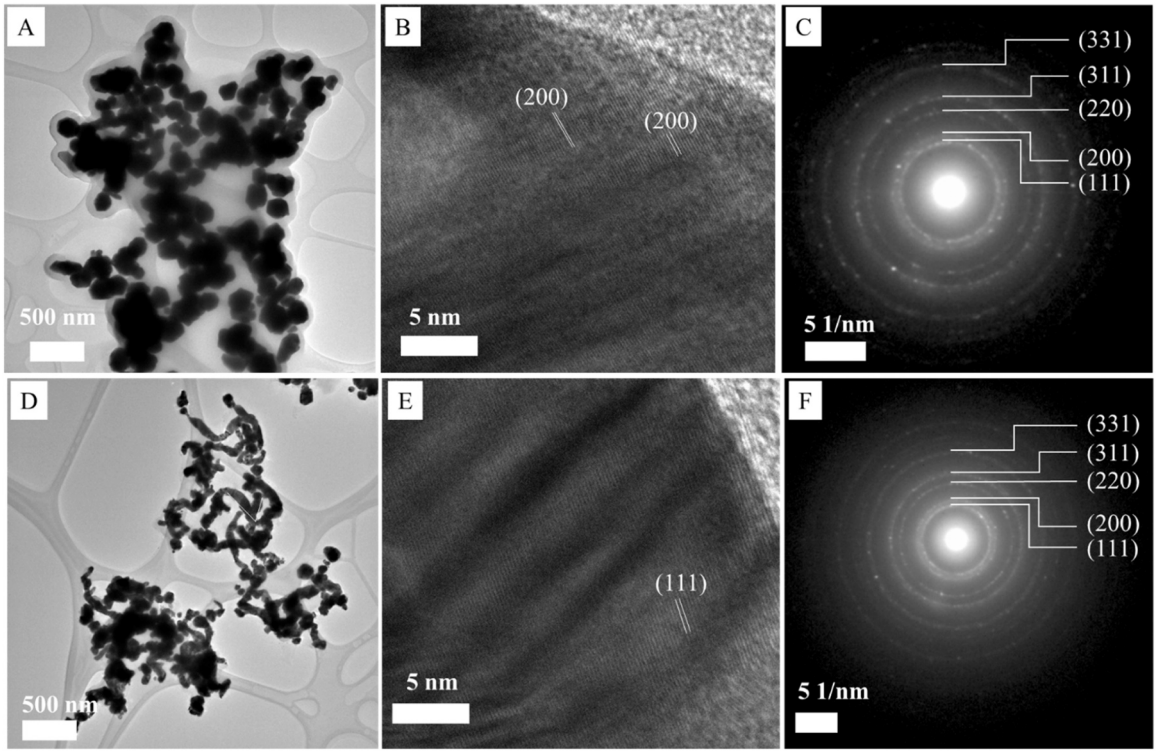

Fig. 4. TEM images of L5AS_AgNP0.91 (A, B, D) and L5AS_AgNP3.61 (C and F) and selected area diffraction of L5AS_AgNP2 (E).

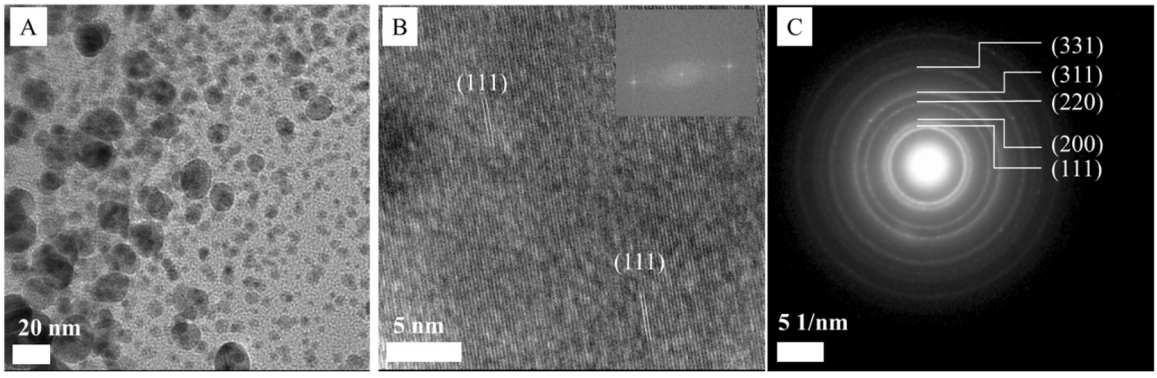

Fig. 5. TEM images (A/B) and SAED (C) of LAPA_AgNP3.61.

overlapped each other. Besides, the sugar ligands might also undergo crystallization on the AgNPs since the interplanar distance (0.330 nm, Fig. 6**B**) did not meet with known interplanar distances of either face centric cubic crystalline structure or hexagonally packed crystalline structure. This is assigned to silver oxide nanoparticles, and it is known that silver oxide layers can form on AgNPs (Kumar et al., 2021). It is possible that the AgNP-GCs possess some silver oxide layers since there was heat treatment and same sugar ligands were used.

The average size of GODA_AuNPs overwhelmingly fell into 87 ± 13 nm range, but some reached up to 170 nm or down to ~35 mm. GODA_AuNPs were in the form of nanoclusters formed from smaller nanoparticles (~ 9 ± 3 nm). At higher magnification, no crystal planes were observed, which can be attributed to low crystallinity of GODA_AuNPs. In contrast to this, L5AS_AuNP gave a very distinct morphology as spherical with a 9–12 nm range and highly crystalline (Fig. 7). The measured interplanar distances (between 0.232 and 0.24 nm) showed that L5AS_AuNPs have *fcc* crystal structure as expected from the sugar ligand synthesized AuNPs (Sancak et al., 2023b). From the literature, SAED and XRD results show compatibility for the sugar ligand synthesized gold and silver nanoparticles, so XRD studies were not performed.

Fig. 8 reveals *in situ* synthesized AgNP-GCs on the scoured cotton fabrics gave high-load and relatively homogenous presence of AgNP-GCs (plain sCF surface is quite smooth) while drop-casting of the AgNP-GCs on plain sCFs and Cysteine modified sCFs did not allow even distribution and high AgNP presence (Figure S6). L5AS_AgNP-GCs on sCF gave 69.6 nm average sized AgNPs and mostly localized between 64 and 110 nm range with spherical to quasispherical morphology while LSA_AgNP-GCs were overwhelmingly nanorod-like structures with 141.1 nm average size and mostly in 80–100 nm range while some reached up to 700 nm. LAPA_AgNP-GCs were spherical, quasispherical, hexagonal and pentagonal with 97.5 nm average size (mostly localized in 60–110 nm range) (Fig. 8). In contrast to these, only L5AS_AuNP-GCs on the sCFS gave dispersed AuNPs with 57.8 nm average size and mostly fell into 42–68 nm range. However, LSA_AuNP-GCs, GODA_AuNP-GCs and LAPA_AuNP-GCs on the sCFs gave more film-like structures and covered the surfaces, for which 18–48 nm ranges, ~ 55 nm and ~ 20 nm were most common size ranges. Particularly, LSA_AuNP-GCs and

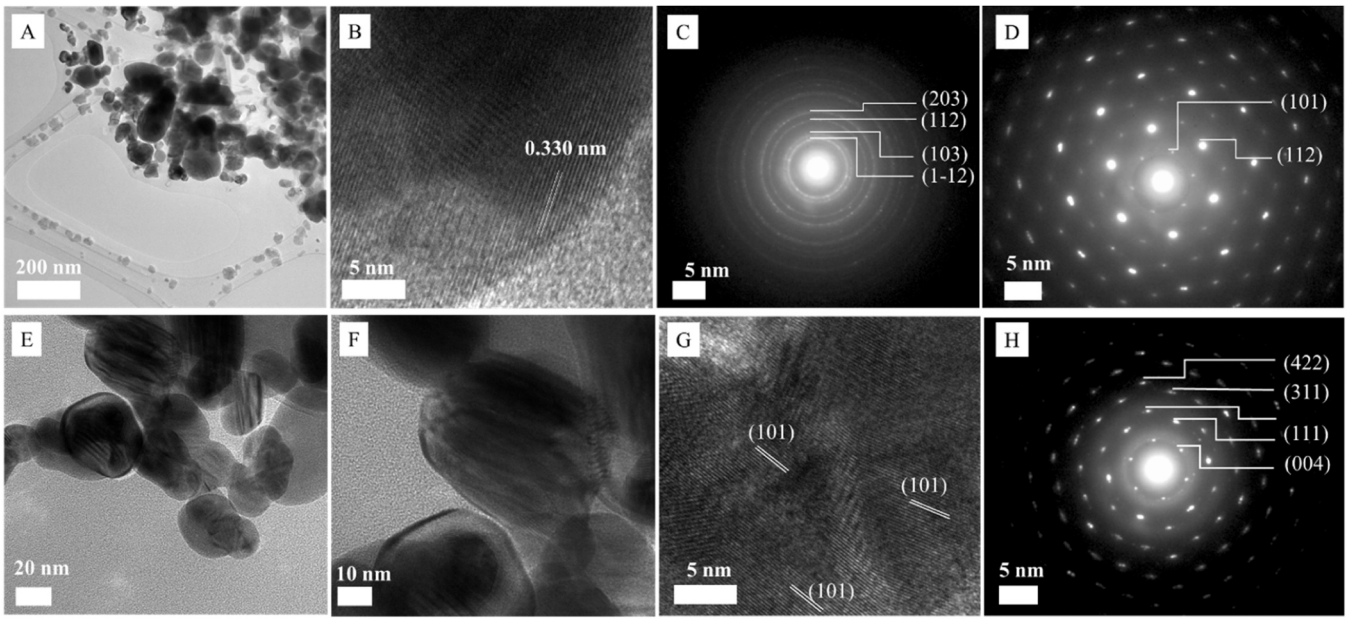

Fig. 6. TEM images and SAEDs of LSA_AgNP3.61 (A/B and C/D) and LSA_AgNP0.45 (E-G and H).

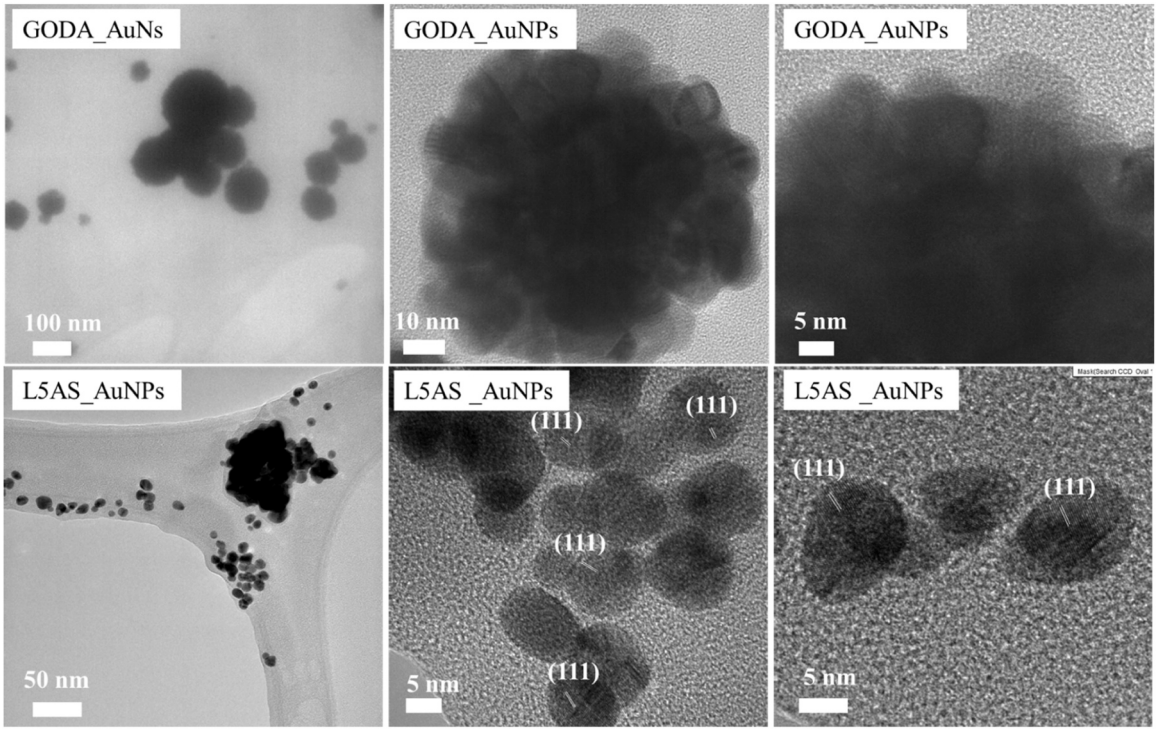

Fig. 7. TEM images of GODA_AuNPs and L5AS_AuNPs.

LAPA_AgNP-GC seem to be that smaller nanoparticles agglomerate to form larger chunks on the fabric surface. In the light of literature (Zhu et al., 2021), AgNPs *in situ* synthesized on cotton fabrics do not agglomerate due to the presence of excess hydroxylic groups, which did not work for all the AuNPs. Therefore, it can be proposed that the carbohydrate ligands LSA and LAPA interactions with AuNPs were quite strong, so the hydroxylic groups could not show their capping character, which is critical in the prevention of agglomeration (Alamer and Beyari, 2022). For the AuNPs, donor-acceptor interactions are critical to prevent AuNPs agglomeration. Therefore, it is possible that the used LSA and LAPA ligand concentrations were higher than that of the optimum concentration (Mehravani et al., 2021). Size and/or morphological differences between the colloidal and *in situ* synthesized AgNP-GCs and AuNP-GCs could be related to the heat treatment, or the cotton fabric altered the ligand-metal ion interaction. EDX analysis showed that the structures on the sCFs were silver (Figure S7) and gold (Figure S8), which revealed that the synthesis was successful. Besides, BET studies revealed that there was nearly no difference for the AgNP-sCFs and the control, which means that AgNPs mostly formed on the cotton fabrics, and they did not serve as fillers under the experimental conditions.

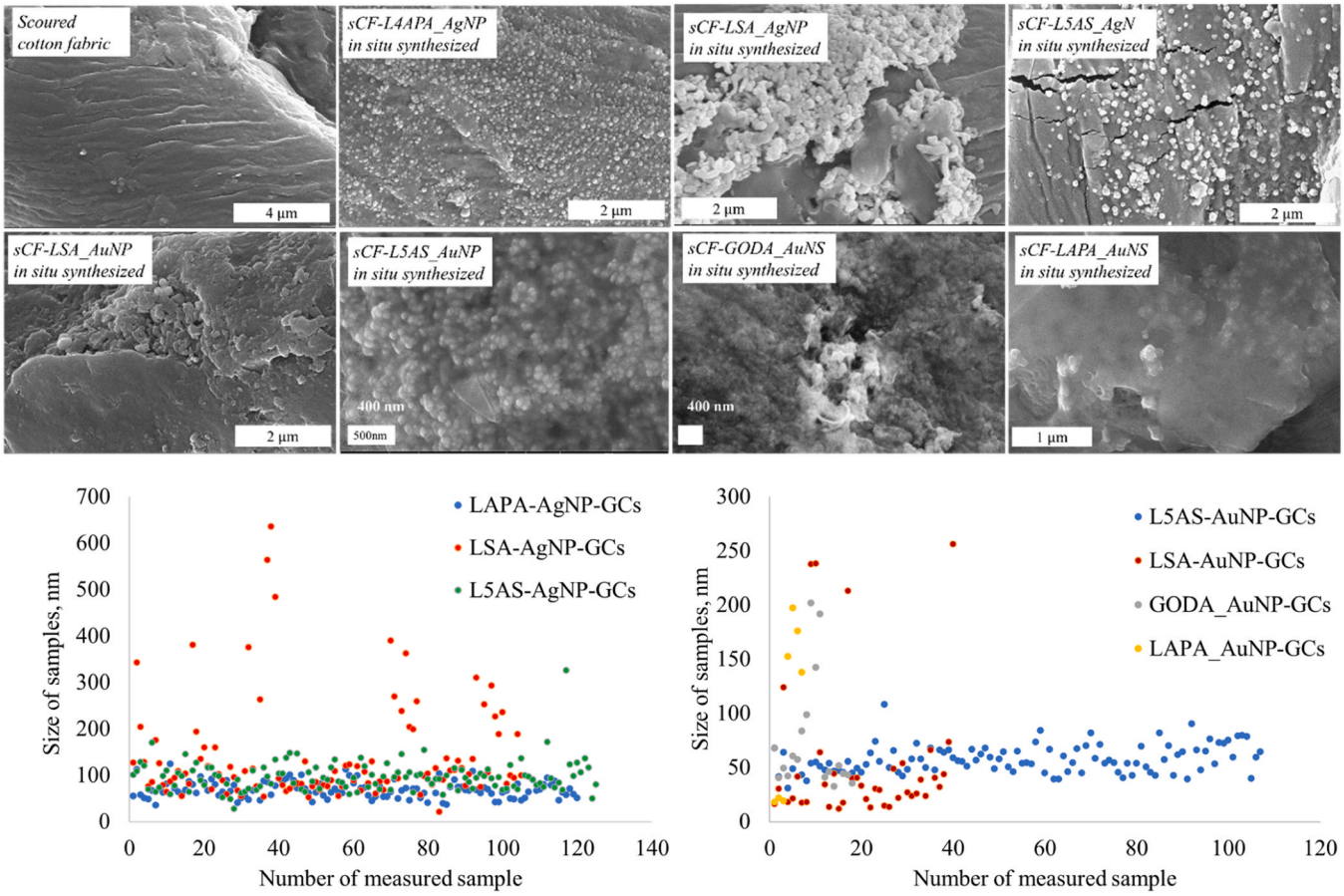

Fig. 8. SEM images of the scoured cotton fabric, nanoparticle-sCFs and their size distribution.

3.3. Antibacterial characterization

As seen from Fig. 9 and Table 1, L5AS_AgNP1 and LAPA_AgNP1 gave relatively lower antibacterial activity for the three bacterial species while L5AS_AgNP4 did not give any antibacterial activity even at 1.26 µg/mL concentration. LSA_AgNP5 gave the highest antibacterial activity against all the tested bacterial species. Besides, LSA_AgNP1 also showed strong antibacterial activity against *P. aeruginosa* and *E. coli* while it showed good antibacterial activity against *S. epidermidis* species. Similarly, the colloidal AgNP-GCs showed strong growth suppression and inhibition of biofilm formation for *K. pneumoniae* (Figure S9).

No bacterial growth was seen with bare-eye for the AgNP-GC-sCFs formulations while illumination revealed that there were some bacterial colonies on and under LSA_AgNP/sCF formulation while there was no illumination for LAPA_AgNP-sCF and L5AS_AgNP-sCF formulations. In the case of Colistin functionalized AuNP-GC-sCFs, illumination did not provide any useful result due to the fact that excess *P. aeruginosa* growth (the fluorescent products spread around) (Fig. 9). In the case of *E. coli*, *S. epidermidis* and *K. pneumoniae*, LAPA_AgNP-sCF and L5AS_AgNP-sCF formulations suppressed all the growth while the AuNP-GC-sCFs did not provide 100 % growth for Colistin resistant *K. pneumoniae* (Figure S9). Propagation of the rinsed NP-sCFs formulations from *P. aeruginosa* samples revealed that LSA_AgNP-sCF, LAPA_AgNP-sCF, L5AS_AgNP-sCF, GODA_AuNP-sCF-C, L5AS_AuNP-sCF-C, and LAPA_AuNP-sCF-C, LSA_AuNP-sCF-C 12 %, 5 %, 1 %, 1 %, 1 %, 2 % and 4 % bacterial growth in comparison to the control cotton fabric. So, this means that *P. aeruginosa* could penetrate into the formulated cotton fabrics and even form films. Interestingly, free colloidal LSA_AgNPs showed higher antibacterial activity while the lowest antibacterial activity for the AgNP-sCFs were obtained for the LSA_AgNP-GC-sCF formulation, which could be related to that Ag^+ release can be lessened by the formulation.

Fig. 10 reveals that GODA_AuNPs interacted with *P. aeruginosa* while L5AS_AuNPs did not give the interaction. GODA_AuNPs and L5AS_AuNPs possess + 34 mV and −34 mV, respectively (the measurements were done triple using Zetasizer, Malvern Panalytical).

AgNPs are potentially toxic to microorganisms, which was shown by *in vitro* and *in vivo* studies (Baveloni et al., 2025). Colloidal AgNPs follow distinct mechanisms to prevent bacterial growth including release of Ag^+ ion, penetration into cytoplasm that results in oxidative stress, disintegration of cellular membrane's integrity and interfering with key proteins and nuclear material (Bruna et al., 2021). The AgNPs impregnated onto the cotton fabric relies on Ag^+ release (Tahir et al., 2024) that can cause DNA damage and reactive oxygen species (ROS) production within bacterium (e.g. *P. aeruginosa*) (Linh et al., 2022). Besides, the hydrophobicity of AgNP-cotton fabric is also critical for bacterial attachment to the surface that also brings an indirect antibacterial activity (Linh et al., 2022). It should be noted that bacterial species can gain resistance to AgNPs (Jain et al., 2022) while the differences between the antibacterial efficacy of AgNP-Cotton fabrics for different bacterial species are not related to the any resistance, rather it is related to the sugar ligand used in the synthesis of AgNPs. Therefore, it is possible to speculate that capture of the bacterial cells on the cotton fabrics through carbohydrate-lectin interactions played roles in addition to the release of Ag^+ ions. In contrast to the AgNP-cotton fabrics, Colistin functionalized AuNP-sCFs brought out the major antibacterial activity by the presence of Colistin. Drastic differences between the bacterial responses to the Colistin functionalized sCFs could be related to two major parameters including (i) the degree of Colistin resistance of the bacterial species and (ii) bacterial interaction with the carbohydrate

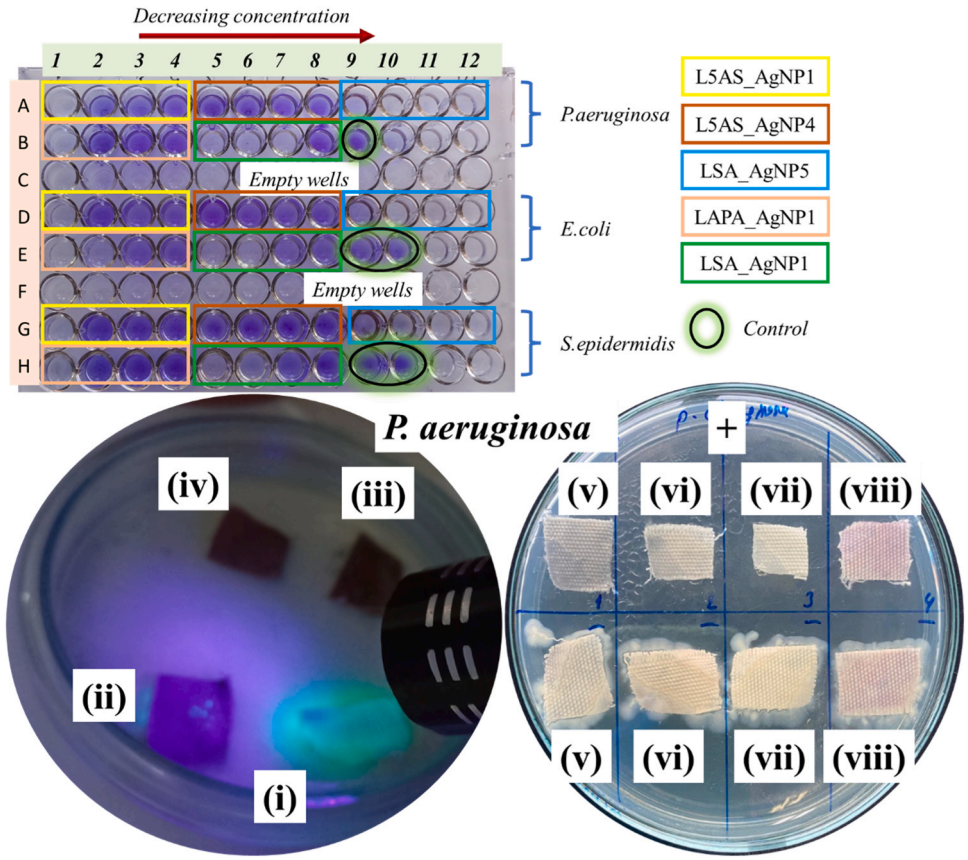

Fig. 9. Antibacterial activity of AgNPs (a) and nanoparticle enhanced cotton fabric (b). i: Control; ii: LSA_AgNP-sCF; iii: LAPA_AgNP-sCF; iv: L5AS_AgNP-sCF; v: GODA_AuNP-sCF; vi: L5AS_AuNP-sCF; vii: LAPA_AuNP-sCF; viii: LSA_AuNP-sCF and + refers to the presence of Colistin (100 ng/cm^2) (C).

Table 1
MIC and MBC values of the AgNPs on *P. aeruginosa*, *E. coli*, *S. epidermidis* and *K. pneumoniae*.

Nanoparticle	MBC/MIC values (μg/mL)			
	P. aeruginosa	*E. coli*	*S. epidermidis*	*K. pneumoniae*
L5AS_AgNP1	0.634/0.634	0.634/ 0.634	0.634/0.634	0.317/0.317
L5AS_AgNP4	Not available	Not available	Not available	Not available
LSA_AgNP5	0.078/0.039	0.078/ 0.039	0.078/0.039	0.078/0.078
LAPA_AgNP1	0.634/0.634	0.634/ 0.634	Not available/ 0.634	0.634/0.317
LSA_AgNP1	0.158/0.079	0.158/ 0.158	0.317/0.158	0.317/0.158

derivative on the surface. Overall, this study shows that decoration of fabric surfaces with carbohydrate derivative synthesized AgNPs or antibiotic functionalized AuNPs could bring semi-selective and strong antibacterial activity.

It is also noteworthy to mention that this study has some limitations including (i) Ag^+ ion release from AgNPs synthesized with different sugar ligands and (ii) formation of silver oxide phases on the metallic AgNPs that might affect the antibacterial activity were not characterized. Besides (iii) wettability of the surfaces (which can affect bacterial attachment), (iv) SEM imaging of bacteria treated cotton fabric formulations to show capture of bacterial cells and formation of bacterial biofilms and (v) the degree of Colistin resistance for each bacterial cells need characterization to provide a deeper understanding of the observed semi-selective antibacterial activity.

4. Conclusion

In situ synthesis of metallic AgNPs and AuNPs on/in scoured cotton fabrics provide homogeneous surfaces in comparison to that administration of the nanoparticles on scoured cotton fabric either predated with Cysteine or not. Silver nanoparticle glycoconjugates and *in situ* synthesized AgNP-GC-sCFs and Colistin functionalized AuNP-GC-sCFs showed excellent anti *P. aeruginosa* activity, and similarly colloidal AgNP-GCs showed none-selective strong antibacterial activity for gram (-) *E. coli, K. pneumoniae* and gram (+) *S. epidermidis*. The study not only shows AgNP-GCs on sCFs can be highly noxious to pathogens, but also it shows Colistin functionalization on AuNP-GCs on sCFs can be toxic to the antibiotic-resistant species. So, these findings can call for further research on surface design using carbohydrate ligands that can target bacterial species through their surface lectins in order to overcome resistance in the development of biomedical coating materials. Besides it is also critical to understand how exactly the surfaces played roles for the semi-selective antibacterial activity, which should be paid attention since biomedical coating materials are critical in order to prevent hospital acquired infections.

CRediT authorship contribution statement

Kırbay Fatma Öztürk: Investigation, Funding acquisition, Formal analysis, Data curation. **Küçük Ardanur:** Writing – original draft, Investigation, Funding acquisition, Formal analysis. **Hafize Dilek Tepe:** Investigation, Formal analysis. **Kasemets Kaja:** Writing – review & editing, Supervision, Investigation, Funding acquisition, Conceptualization. **Sancak Sedanur:** Writing – original draft, Investigation, Formal analysis. **Otsus Maarja:** Methodology, Investigation, Formal analysis. **Güney Şevval:** Investigation, Formal analysis, Data curation. **Sel**

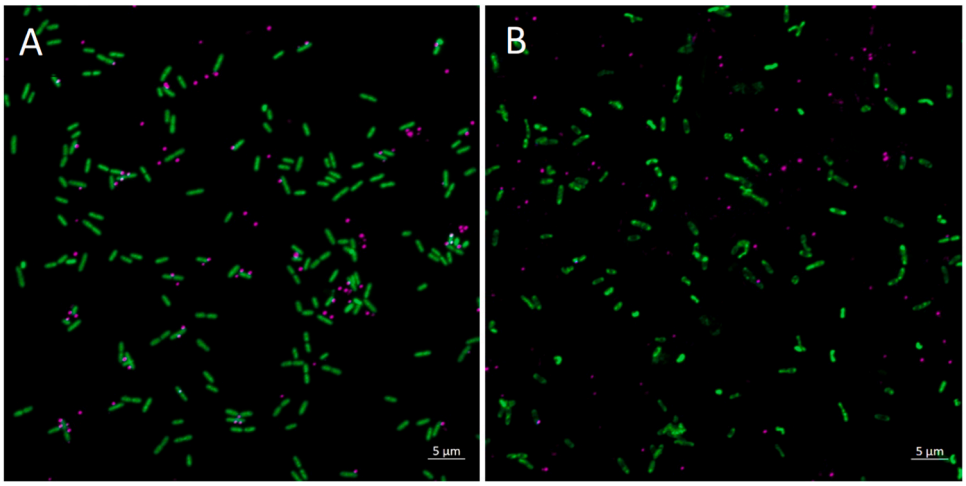

Fig. 10. Confocal laser scanning microscopy image of GODA_AuNPs (A) and L5AS_AuNPs (B) interactions with bacteria *P. aeruginosa*. Cells were stained by green-fluorescent stain Syto 9, and AuNPs were visualized by reflection mode at 640 nm (purple dots). All scale bars are 5 µm.

Sedanur: Investigation, Formal analysis, Data curation. **Kılınç Çetin:** Writing – review & editing, Validation, Supervision, Software, Formal analysis, Conceptualization. **Taşdelen Zehra:** Investigation, Formal analysis, Data curation. **Esinti İrem Demirbaş:** Investigation, Formal analysis, Data curation. **yazgan idris:** Writing – review & editing, Writing – original draft, Supervision, Investigation, Funding acquisition, Formal analysis, Data curation, Conceptualization.

Declaration of Competing Interest

The authors declare no conflict of interest.

Acknowledgements

The authors acknowledge TUBİTAK 2209 Student Projects of Türkiye (Grant number 1919B012109406), Kastamonu University Internal Grant (Türkiye, Grant number KÜBAP-01/2022–20), the COST Action CA21145-(EURESTOP) (European Cooperation in Science and Technology, European Network for diagnosis and treatment of antibiotic-resistant bacterial infections, Bruxelles-Belgium), Fatma Öztürk Kırbay personally thanks to 2218 TUBITAK National Postdoctoral Research Fellowship Program 2021/2 of Türkiye, and Estonian Research Council Project PRG749.

Appendix A. Supporting information

Supplementary data associated with this article can be found in the online version at doi:10.1016/j.microb.2025.100269.

Data availability

Data will be made available on request.

References

Burkatovskaya, M., Castano, A.P., Demidova-Rice, T.N., Tegos, G.P., Hamblin, M.R., 2008. Effect of chitosan acetate bandage on wound healing in infected and noninfected wounds in mice. Wound Repair Regen. 16, 425–431. https://doi.org/10.1111/j.1524-475X.2008.00382.x.

Wang, Y., Yang, Y., Shi, Y., Song, H., Yu, C., 2020. Antibiotic-free antibacterial strategies enabled by nanomaterials: progress and perspectives. Adv. Mater. 32, 1–21. https://doi.org/10.1002/adma.201904106.

Wounds, B.I., Nowak, M., 2021. Nanomaterials as a successor of antibiotics in. MDPI Antibiot. 10, 941.

Khan, S.U., Saleh, T.A., Wahab, A., Khan, M.H.U., Khan, D., Khan, W.U., Rahim, A., Kamal, S., Khan, F.U., Fahad, S., 2018. Nanosilver: New ageless and versatile biomedical therapeutic scaffold. Int. J. Nanomed. 13, 733–762. https://doi.org/10.2147/IJN.S153167.

Yin, I.X., Zhang, J., Zhao, I.S., Mei, M.L., Li, Q., Chu, C.H., 2020. The antibacterial mechanism of silver nanoparticles and its application in dentistry. Int. J. Nanomed. 15, 2555–2562.

Pareek, V., Devineau, S., Sivasankaran, S.K., Bhargava, A., Panwar, J., Srikumar, S., Fanning, S., 2021. Silver nanoparticles induce a triclosan-like antibacterial action mechanism in multi-drug resistant klebsiella pneumoniae. Front. Microbiol. 12, 1–12. https://doi.org/10.3389/fmicb.2021.638640.

Zhang, Y., Pan, X., Liao, S., Jiang, C., Wang, L., Tang, Y., Wu, G., Dai, G., Chen, L., 2020. Quantitative proteomics reveals the mechanism of silver nanoparticles against multidrug-resistant pseudomonas aeruginosa biofilms. J. Proteome Res. 19, 3109–3122. https://doi.org/10.1021/acs.jproteome.0c00114.

El-Shishtawy, R.M., Asiri, A.M., Abdelwahed, N.A.M., Al-Otaibi, M.M., 2011. In situ production of silver nanoparticle on cotton fabric and its antimicrobial evaluation. Cellulose 18, 75–82. https://doi.org/10.1007/s10570-010-9455-1.

Sarma, P.P., Rai, A., Baruah, P.K., 2024. Recent advances in the development of antibiotics-coated gold nanoparticles to combat antimicrobial resistance. Antibiotics 13, 124. https://doi.org/10.3390/antibiotics13020124.

Ullah, R., Hameed, A., Azam, A., Aziz, T., Farhan, Qiao, S., 2022a. Facile synthesis of silver and gold nanoparticles using chicken feather extract as template and their biological applications. Biomass. Convers. Biorefinery 14, 28133–28141. https://doi.org/10.1007/s13399-022-03447-4.

Ullah, R., Azam, A., Aziz, T., Farhan, Rehman, H.U., Qiao, S., Hameed, A., 2022b. Peacock feathers extract use as template for synthesis of Ag and Au nanoparticles and their biological applications. Waste Biomass-.-. Valoriz. 13, 659–666. https://doi.org/10.1007/s12649-021-01537-4.

Ghosh, J., 2021. Development of antimicrobial and wound healing properties on cotton medical bandage by using the extract of eco-friendly herbs. J. Inst. Eng. Ser. E 102, 75–86. https://doi.org/10.1007/s40034-020-00199-6.

İpek, Y., Ertekin, Ö., 2021. Developing antibacterial cotton fabric with zinc borate impregnation process. Fibers Polym. 22, 2826–2833. https://doi.org/10.1007/s12221-021-0670-1.

Chen, M., ShangGuan, J., Jiang, J., Jiang, J., Li, F., Dong, Q., Diao, H., Liu, X., 2023a. Durably antibacterial cotton fabrics coated by protamine via Schiff base linkages. Int. J. Biol. Macromol. 227, 1078–1088. https://doi.org/10.1016/j.ijbiomac.2022.11.287.

Chen, F., Tian, Q., Wang, T., Ma, L., Liu, R., Wang, S., 2023b. Fabrication of a multifunctional antibacterial Cotton-based fabric for personal cooling. Appl. Surf. Sci. 609, 155291. https://doi.org/10.1016/j.apsusc.2022.155291.

Gokce, Y., Aktas, Z., Capar, G., Kutlu, E., Anis, P., 2020. Improved antibacterial property of cotton fabrics coated with waste sericin/silver nanocomposite. Mater. Chem. Phys. 254, 123508. https://doi.org/10.1016/j.matchemphys.2020.123508.

Li, Y., Wang, P., Chen, M., Chen, J., Huang, W., Xiang, S., Zhao, S., Fu, F., Liu, X., 2023. A facile and scalable strategy for constructing Janus cotton fabric with persistent antibacterial activity. Int. J. Biol. Macromol. 236, 123946. https://doi.org/10.1016/j.ijbiomac.2023.123946.

Knežević, M., Kramar, A., Hajnrih, T., Korica, M., Nikolić, T., Žekić, A., Kostić, M., Knežević, M., Kramar, A., Hajnrih, T., Korica, M., 2022. Influence of potassium permanganate oxidation on structure and properties of cotton influence of potassium permanganate oxidation on structure and properties of cotton. J. Nat. Fibers 19, 403–415. https://doi.org/10.1080/15440478.2020.1745120.

Chung, C., Lee, M., Kyung, E., 2004. Characterization of cotton fabric scouring by FT-IR ATR spectroscopy. Carbohydr. Polym. 58, 417–420. https://doi.org/10.1016/j.carbpol.2004.08.005.

Dang, X., Li, N., Yu, Z., Ji, X., Yang, M., Wang, X., 2024. Advances in the preparation and application of cellulose-based antimicrobial materials: a review. Carbohydr. Polym. 342, 122385. https://doi.org/10.1016/j.carbpol.2024.122385.

Gulati, R., Sharma, S., Sharma, R.K., 2022. Antimicrobial textile: recent developments and functional perspective. Polym. Bull. 79, 5747–5771. https://doi.org/10.1007/s00289-021-03826-3.

Khan, F.U., Asimullah, Khan, S.B., Kamal, T., Asiri, A.M., Khan, I.U., Akhtar, K., 2017. Novel combination of zero-valent Cu and Ag nanoparticles @ cellulose acetate nanocomposite for the reduction of 4-nitro phenol. Int. J. Biol. Macromol. 102, 868–877. https://doi.org/10.1016/j.ijbiomac.2017.04.062.

Raw, N., Fiber, C., 2023. Washable antimicrobial wipes fabricated from a blend of nanocomposite raw cotton fiber. MDPI Mol. 28, 1051.

Soleimani-Gorgani, A., Avinc, O., Alborz, R., 2023. Sustainable antibacterial cotton fabrics with in situ formed silver nanoparticles by bio-inkjet printing. J. Clean. Prod. 386, 135796. https://doi.org/10.1016/j.jclepro.2022.135796.

Nosheen, A., Khalid, M., Manzoor, S., Ashraf, M., Xue, Z., Akram, S., Khan, D.S., Urooj, S., Hashmi, A.H., 2022. Pilot-scale production of highly durable bioactive and UV-protective cotton fabric by electroless deposition of copper oxide on cotton fabric. Cellulose 30, 2573–2595. https://doi.org/10.1007/s10570-022-05009-3.

Attia, N.F., Mohamed, A., Hussein, A., El-Demerdash, A.G.M., Kandil, S.H., 2023. Greener bio-based spherical nanoparticles for efficient multilayer textile fabrics nanocoating with outstanding fire retardancy, toxic gases suppression, reinforcement and antibacterial properties. Surf. Interfaces 36, 102595. https://doi.org/10.1016/j.surfin.2022.102595.

Mast, J., Van Miert, E., Siciliani, L., Cheyns, K., Blaude, M., Wouters, C., Waegeneers, N., Bernsen, R., Vleminckx, C., Van Loco, J., Verleysen, E., 2023. Application of silver-based biocides in face masks intended for general use requires regulatory control. Sci. Total Environ. 870, 161889. https://doi.org/10.1016/j.scitotenv.2023.161889.

Shehabeldine, A.M., Hashem, A.H., Wassel, A.R., Hasanin, M., 2022. Antimicrobial and antiviral activities of durable cotton fabrics treated with nanocomposite based on zinc oxide nanoparticles, acyclovir, nanochitosan, and clove oil. Appl. Biochem. Biotechnol. 194, 783–800. https://doi.org/10.1007/s12010-021-03649-y.

Wang, S., Feng, Y., Jia, X., Ma, X., Chen, W., Yang, L., Li, J., 2024. Cotton fiber-based dressings with wireless electrical stimulation and antibacterial activity for wound repair. Int. J. Biol. Macromol. 256, 128496. https://doi.org/10.1016/j.ijbiomac.2023.128496.

Qi, H., Yang, L., Ma, R., Xiang, Y., Dai, Y., Ren, J., Bin Xu, B., El-Bahy, Z.M., Thabet, H.K., Huang, Z., Ben, W., Yu, H., Guo, Z., 2024. Amoxicillin-laded sodium alginate/cellulose nanocrystals/polyvinyl alcohol composite nanonetwork sponges with enhanced wound healing and antibacterial performance. Int. J. Biol. Macromol. 280, 135701. https://doi.org/10.1016/j.ijbiomac.2024.135701.

Muhammad, A., Kidanemariam, A., Lee, D., Duong Pham, T.T., Park, J., 2024. Durability of antimicrobial agent on nanofiber: a collective review from 2018 to 2022. J. Ind. Eng. Chem. 130, 1–24. https://doi.org/10.1016/j.jiec.2023.09.032.

AbdElhady, M.M., 2012. Preparation and characterization of chitosan/zinc oxide nanoparticles for imparting antimicrobial and UV protection to cotton fabric. Int. J. Carbohydr. Chem. 2012, 1–6. https://doi.org/10.1155/2012/840591.

Nanoparticles, C.O., 2020. Antibacterial cotton fabric functionalized with copper oxide nanoparticles. molecules 25, 5802. https://doi.org/10.3390/molecules25245802.

Wang, Y., Liu, K.K., Zhao, W.B., Sun, J.L., Chen, X.X., Zhang, L.L., Cao, Q., Zhou, R., Dong, L., Shan, C.X., 2023. Antibacterial fabrics based on synergy of piezoelectric effect and physical interaction. Nano Today 48, 101737. https://doi.org/10.1016/j.nantod.2022.101737.

Gao, D., Li, X., Li, Y., Lyu, B., Ren, J., 2021. Long-acting antibacterial activity on the cotton fabric. Cellulose 28, 1221–1240. https://doi.org/10.1007/s10570-020-03560-5.

El-Naggar, M.E., Shaarawy, S., Abdel-Aziz, M.S., Abd El Moneim katry, H., Youssef, A.M., 2022. Functionalization of cotton fabrics with titanium oxide doped silver nanoparticles: Antimicrobial and UV protection activities. Luminescence 37, 854–864. https://doi.org/10.1002/bio.4229.

Hu, L., Han, H., Xu, Z., Hou, X., Wang, F., Song, K., 2024. Multimodal integrated and broadband light-driven antibacterial cellulose fabric based on π-π coupling enhanced intermolecular FRET. Int. J. Biol. Macromol. 277, 134466. https://doi.org/10.1016/j.ijbiomac.2024.134466.

Wu, L., Fan, B., Yan, B., Liu, Y., Yu, Y., Cui, L., Zhou, M., Wang, Q., Wang, P., 2024. Construction of durable antibacterial cellulose textiles through grafting dynamic disulfide-containing amino-compound and nanosilver deposition. Int. J. Biol. Macromol. 259, 129085. https://doi.org/10.1016/j.ijbiomac.2023.129085.

Anwar, Y., Ullah, I., Ul-Islam, M., Alghamdi, K.M., Khalil, A., Kamal, T., 2021. Adopting a green method for the synthesis of gold nanoparticles on cotton cloth for antimicrobial and environmental applications. Arab. J. Chem. 14, 103327. https://doi.org/10.1016/j.arabjc.2021.103327.

Pina-Sánchez, M., Rua, M., Del Pozo, J.L., 2023. Present and future of resistance in Pseudomonas aeruginosa: implications for treatment. Rev. Esp. Quimioter. 36, 54–58. https://doi.org/10.37201/req/s01.13.2023.

Belgin, S., Öz, V., 2017. Pseudomonas aeruginosa: characteristics and quorum sensing mechanism. J. Food Feed Sci. 18, 42–52.

Azam, M.W., Khan, A.U., 2019. Updates on the pathogenicity status of Pseudomonas aeruginosa. Drug Discov. Today 24, 350–359. https://doi.org/10.1016/j.drudis.2018.07.003.

Behzadi, P., Baráth, Z., Gajdács, M., 2021. It's not easy being green: A narrative review on the microbiology, virulence and therapeutic prospects of multidrug-resistant pseudomonas aeruginosa. Antibiotics 10, 1–29. https://doi.org/10.3390/antibiotics10010042.

Hu, X.Le, Chu, L., Dong, X., Chen, G.R., Tang, T., Chen, D., He, X.P., Tian, H., 2019. Multivalent glycosheets for double light–driven therapy of multidrug-resistant bacteria on wounds. Adv. Funct. Mater. 29, 1806986. https://doi.org/10.1002/adfm.201806986.

Yu, G., Vicini, A.C., Pieters, R.J., 2019. Assembly of divalent ligands and their effect on divalent binding to pseudomonas aeruginosa lectin LecA. J. Org. Chem. 84, 2470–2488. https://doi.org/10.1021/acs.joc.8b02727.

Sommer, R., Exner, T.E., Titz, A., 2014. A biophysical study with carbohydrate derivatives explains the molecular basis of monosaccharide selectivity of the Pseudomonas aeruginosa lectin lecB. PLoS One 9, e112822. https://doi.org/10.1371/journal.pone.0112822.

Pertici, F., Pieters, R.J., 2012. Potent divalent inhibitors with rigid glucose click spacers for Pseudomonas aeruginosa lectin LecA. Chem. Commun. 48, 4008–4010. https://doi.org/10.1039/c2cc30234a.

Loris, R., Tielker, D., Jaeger, K.E., Wyns, L., 2003. Structural basis of carbohydrate recognition by the lectin LecB from Pseudomonas aeruginosa. J. Mol. Biol. 331, 861–870. https://doi.org/10.1016/S0022-2836(03)00754-X.

Yaman Turan, N., Korcan, E., Aydin, B., 2024. Comparing the antimicrobial properties of propolis and silver particle-doped cotton fabric. Cellulose 31, 3259–3273. https://doi.org/10.1007/s10570-024-05790-3.

Elias, R., Duarte, A., Perdigão, J., 2021. A molecular perspective on colistin and Klebsiella pneumoniae: mode of action, resistance genetics, and phenotypic susceptibility. Diagnostics 11, 1165. https://doi.org/10.3390/diagnostics11071165.

Kumar, S., Majhi, R.K., Singh, A., Mishra, M., Tiwari, A., Chawla, S., Guha, P., Satpati, B., Mohapatra, H., Goswami, L., Goswami, C., 2019. Carbohydrate-coated gold-silver nanoparticles for efficient elimination of multidrug resistant bacteria and in vivo wound healing. ACS Appl. Mater. Interfaces 11, 42998–43017. https://doi.org/10.1021/acsami.9b17086.

Yiğit, İ., Eren, S., Karalı, R., Yıbar, M.F., Eren, H.A., 2021. Comparison of the colour fading effects of sodium hypochlorite and ozone treatments. Color. Technol. 137, 615–624. https://doi.org/10.1111/cote.12554.

Rezaee, R., Montazer, M., Mianehro, A., Mahmoudirad, M., 2021. Biomedical applicable cellulose fabric modified with zirconium-based metal-organic frameworks (Zr-MOFs). Starch 73, 2100120. https://doi.org/10.1002/star.202100120.

Saladino, G.M., Hamawandi, B., Demir, M.A., Yazgan, I., Toprak, M.S., 2021. A versatile strategy to synthesize sugar ligand coated superparamagnetic iron oxide nanoparticles and investigation of their antibacterial activity. Colloids Surf. A Physicochem. Eng. Asp. 613, 126086. https://doi.org/10.1016/j.colsurfa.2020.126086.

Jeong, H.S., Adachi, K., Bong, K.L., Dong, G.K., Yeon, K.K., Kyoung, R.K., Hea, Y.L., Kawai, T., Hyung, J.C., 2007. Facile and rapid direct gold surface immobilization with controlled orientation for carbohydrates. Bioconj. Chem. 18, 2197–2201. https://doi.org/10.1021/bc700288z.

Yazgan, I., Gümüş, A., Gökkuş, K., Demir, M.A., Evecen, S., Sönmez, H.A., Miller, R.M., Bakar, F., Oral, A., Popov, S., Toprak, M.S., 2020. On the effect of modified carbohydrates on the size and shape of gold and silver nanostructures. Nanomaterials 10, 1–17. https://doi.org/10.3390/nano10071417.

Yazgan, I., Osonga, F.J., Miller, R.M., Kariuki, V.M., Zhang, J., Feng, J., Skeete, Z., Crapo, H., Schulte, J., Sadik, O.A., 2021. Greener one-pot synthesis of gold nanoparticle glycoconjugates using functionalized sugars. ACS Agric. Sci. Technol. 1, 379–389. https://doi.org/10.1021/acsagscitech.1c00093.

Sancak, S., Yazgan, İ., Bayarslan, A.U., Ayna, A., Evecen, S., Taşdelen, Z., Gümüş, A., Sönmez, H.A., Demir, M.A., Demir, S., Bakar, F., Dilek-Tepe, H., Kasemets, K., Otsus, M., Çeter, T., 2023a. Surface chemistry dependent toxicity of inorganic nanostructure glycoconjugates on bacterial cells and cancer cell lines. J. Drug Deliv. Sci. Technol. 79. https://doi.org/10.1016/j.jddst.2022.104054.

Bayisa, T., Edossa, G.D., Gupta, N.K., Inki, L.G., 2023. Antibacterial durability of L-methionine modified cotton fabrics functionalized with ZnO nanoparticles, Sci. African 22 (2023) e01977. https://doi.org/10.1016/j.sciaf.2023.e01977..

Sancak, S., Yazgan, I., Bayarslan, A.U., Ayna, A., Evecen, S., Taşdelen, Z., Gümüş, A., Sönmez, H.A., Demir, M.A., Demir, S., Bakar, F., Dilek-Tepe, H., Kasemets, K., Otsus, M., Çeter, T., 2023b. Surface chemistry dependent toxicity of inorganic nanostructure glycoconjugates on bacterial cells and cancer cell lines. J. Drug Deliv. Sci. Technol. 79, 104054. https://doi.org/10.1016/j.jddst.2022.104054.

Yazgan, İ., 2019. Synthesis of open-chain sugar derivatives as anticancer and antimicrobial agents. Commun. Fac. Sci. Univ. Ank. Ser. C. Biol. 28, 148–159.

Pitch, G.M., Andre, J.S., Davie, A.J., 2015. Investigations of water uptake on sodium acetate trihydrate and nonhydrate as model aerosol surfaces using the DRIFTS And ATR-FTIR techniques, içinde. Proc. Natl. Conf. Undergrad. Res.

Kakihana, M., Nagumo, T., 1987. Assignment for the infrared spectrum of solid sodium propionate from low-temperature measurements in combination with 13C isotopic shifts. Z. fur Naturforsch. - Sect. A J. Phys. Sci. 42, 477–484. https://doi.org/10.1515/zna-1987-0509.

Habka, S., Very, T., Donon, J., Vaquero-Vara, V., Tardivel, B., Charnay-Pouget, F., Mons, M., Aitken, D.J., Brenner, V., Gloaguen, E., 2019. Identification of ion pairs in solution by IR spectroscopy: crucial contributions of gas phase data and simulations. Phys. Chem. Chem. Phys. 21, 12798–12805. https://doi.org/10.1039/c9cp00700h.

Susan Doofan, I., Donald, K., Esther Nguumbur, I., Isaac Gbaa, A., Godwin, I., 2021. Synthesis and spectrophotometric properties of sodium metal carboxylates. Sci. J. Chem. 9, 113. https://doi.org/10.11648/j.sjc.20210905.11.

Hu, D., Liu, L., Chen, W., Li, S., Zhao, Y., 2012. A novel preparation method for 5-aminosalicylic acid loaded eudragit S100 nanoparticles. Int. J. Mol. Sci. 13, 6454–6468. https://doi.org/10.3390/ijms13056454.

Singh, Y.P., Das, R., Singh, R.A., 2007. Numerical simulation of the internal vibrations of COOH group in amino-salicylic acids, 019–023 Afr. J. Biochem. 1. https://doi.org/10.5897/AJBR.9000175.

Wiercigroch, E., Szafraniec, E., Czamara, K., Pacia, M.Z., Majzner, K., Kochan, K., Kaczor, A., Baranska, M., Malek, K., 2017. Raman and infrared spectroscopy of carbohydrates: a review. Spectrochim. Acta Part A Mol. Biomol. Spectrosc. 185, 317–335. https://doi.org/10.1016/j.saa.2017.05.045.

Akkaya, Y., Balci, K., Goren, Y., Akyuz, S., 2015. A vibrational spectroscopy study on 3-aminophenylacetic acid by DFT calculations. Spectrochim. Acta - Part A Mol. Biomol. Spectrosc. 147, 303–315. https://doi.org/10.1016/j.saa.2015.03.094.

Srimathi, M., Rajalakshmi, R., Subhashini, S., 2014. Polyvinyl alcohol-sulphanilic acid water soluble composite as corrosion inhibitor for mild steel in hydrochloric acid medium. Arab. J. Chem. 7, 647–656. https://doi.org/10.1016/j.arabjc.2010.11.013.

Srivastav, G., Yadav, R.K., Yadav, B., Yadav, R.A., 2023. Vibrational spectra and molecular structure of sulfanilic acid: IR and low temperature Raman studies and DFT investigation of monomeric and dimeric forms. J. Mol. Struct. 1272, 134143. https://doi.org/10.1016/j.molstruc.2022.134143.

Rana Tomar, D., Venkatesan Jayakumar, S., 2023. Novel synthetic methodology of Diclofenac derivatives and its spectrochemical studies. Mater. Today Proc. 80, 141–149. https://doi.org/10.1016/j.matpr.2022.11.016.

Ismail, E.H., Sabry, D.Y., Mahdy, H., Khalil, M.M.H., 2014. Synthesis and characterization of some ternary metal complexes of curcumin with 1,10-phenanthroline and their anticancer applications. J. Sci. Res. 6, 509–519. https://doi.org/10.3329/jsr.v6i3.18750.

Colombi, B.L., De Cássia Siqueira Curto Valle, R., Borges Valle, J.A., Andreaus, J., 2021. Advances in sustainable enzymatic scouring of cotton textiles: Evaluation of different post-treatments to improve fabric wettability. Clean. Eng. Technol. 4, 100160. https://doi.org/10.1016/j.clet.2021.100160.

Nateghi, M.R., Hajimirzababa, H., 2014. Effect of silver nanoparticles morphologies on antimicrobial properties of cotton fabrics. J. Text. Inst. 105, 806–813. https://doi.org/10.1080/00405000.2013.855377.

Sadanand, V., Tian, H., Rajulu, A.V., Satyanarayana, B., 2017. Antibacterial cotton fabric with in situ generated silver nanoparticles by one-step hydrothermal method. Int. J. Polym. Anal. Charact. 22, 275–279. https://doi.org/10.1080/1023666X.2017.1287828.

Igarashi, T., Hoshi, M., Nakamura, K., Kaharu, T., Murata, K., 2020. Direct observation of bound water on cotton surfaces by atomic force microscopy and atomic force microscopy – infrared spectroscopy. J. Phys. Chem. C. 14 4196–4201. https://doi.org/10.1021/acs.jpcc.0c00423.

Nikonenko, N.A., Buslov, D.K., Sushko, N.I., Zhbankov, R.G., 2005. Spectroscopic manifestation of stretching vibrations of glycosidic linkage in polysaccharides. J. Mol. Struct. 752, 20–24. https://doi.org/10.1016/j.molstruc.2005.05.015.

Fuller, M., Whiley, H., Köper, I., 2020. Antibiotic delivery using gold nanoparticles. SN Appl. Sci. 2, 1022. https://doi.org/10.1007/s42452-020-2835-8.

Virgen-Ortiz, A., Limón-Miranda, S., Soto-Covarrubias, M.A., Apolinar-Iribe, A., Rodríguez-León, E., 2015. Biocompatible silver nanoparticles synthesized using Rumex hymenosepalus extract decreases fasting glucose levels in diabetic rats. Dig. J. Nanomater. Biostruct. 10, 927–933.

Kumar, I., Yaseen, B., Gangwar, C., Yadav, R., Mishra, S.K., Mohan Naik, R., 2021. Ovalbumin mediated eco-friendly synthesis of silver oxide nanoparticles and their antibacterial and antifungal studies. Mater. Today Proc. 46, 2330–2334. https://doi.org/10.1016/j.matpr.2021.04.403.

Zhu, J., Li, H., Wang, Y., Wang, Y., Yan, J., 2021. Preparation of ag nps and its multifunctional finishing for cotton fabric. Polymers 13, 1338. https://doi.org/10.3390/polym13081338.

Alamer, F.A., Beyari, R.F., 2022. Overview of the Influence of Silver, Gold, and Titanium Nanoparticles on the Physical Properties of PEDOT:PSS-Coated Cotton Fabrics. Nanomaterials 12, 1609. https://doi.org/10.3390/nano12091609.

Mehravani, B., Ribeiro, A.I., Zille, A., 2021. Gold nanoparticles synthesis and antimicrobial effect on fibrous materials. Nanomaterials 11, 1067. https://doi.org/10.3390/nano11051067.

Baveloni, F.G., Meneguin, A.B., Sábio, R.M., de Camargo, B.A.F., Trevisan, D.P.V., Duarte, J.L., de Araújo, J.T.C., Luiz, M.T., Zanatta, M.B.T., da Silva, I.C.P., Barud, H., de Andrade, T.A.M., Menegário, A.A., Bauab, T.M., Chorilli, M., 2025. Antimicrobial effect of silver nanoparticles as a potential healing treatment for wounds contaminated with Staphylococcus aureus in wistar rats. J. Drug Deliv. Sci. Technol. 103, 106445. https://doi.org/10.1016/j.jddst.2024.106445.

Bruna, T., Maldonado-Bravo, F., Jara, P., Caro, N., 2021. Silver nanoparticles and their antibacterial applications. Int. J. Mol. Sci. 22, 7202. https://doi.org/10.3390/ijms22137202.

Tahir, I., Amina, S.J., Ahmed, N.M., Janjua, H.A., 2024. Antimicrobial coating of biologically synthesized silver nanoparticles on surgical fabric and surgical blade to prevent nosocomial infections. Heliyon 10, e35968. https://doi.org/10.1016/j.heliyon.2024.e35968.

Linh, N.T.T., Diep, T.C., Vy, T.T., Dat, N.M., Trinh, D.N., Thinh, D.B., Viet, N.D., Hai, N. D., Huong, L.M., Tinh, N.T., Phong, M.T., Hieu, N.H., 2022. Cotton fabric coated with graphene-based silver nanoparticles: synthesis, modification, and antibacterial activity. Cellulose 29, 6405–6424. https://doi.org/10.1007/s10570-022-04659-7.

Jain, A., Kongkham, B., Puttaswamy, H., Butola, B.S., Malik, H.K., Malik, A., 2022. Development of wash-durable antimicrobial cotton fabrics by in situ green synthesis of silver nanoparticles and investigation of their antimicrobial efficacy against drug-resistant bacteria. Antibiotics 11, 864. https://doi.org/10.3390/antibiotics11070864.